Slide-hold-slide protocols and frictional healing in Discrete Element Method (DEM) simulations of granular fault gouge

Behrooz Ferdowsi[1], **Allan M. Rubin**[1]

[1]Department of Geosciences, Princeton University, Princeton, NJ 08544, USA

Key Points:

- We ran DEM simulations of a sheared granular layer with time-independent contact-scale properties in slide-hold-slide protocols.
- The slide-hold simulations with different model stiffnesses mimic the stress decay response of laboratory friction data.
- As with lab data, the peak stress upon resliding increases linearly with log hold time, with a slope close to the rate-state 'b'.

Corresponding author: Behrooz Ferdowsi, `behrooz@princeton.edu`

Abstract

The empirical constitutive modeling framework of Rate- and State-dependent Friction (RSF) is commonly used to describe the time-dependent frictional response of fault gouge to perturbations from steady sliding. In a previous study (Ferdowsi & Rubin, 2020), we found that a granular-physics-based model of a fault shear zone, with time-independent properties at the contact scale, reproduces the phenomenology of laboratory rock and gouge friction experiments in velocity-step and slide-hold protocols. A few slide-hold-slide simulations further suggested that the granular model might outperform current empirical RSF laws in describing laboratory data. Here, we explore the behavior of the same Discrete Element Method (DEM) model in slide-hold and slide-hold-slide protocols over a wide range of sliding velocities, hold durations, and system stiffnesses, and provide additional support for this view. We find that, similar to laboratory data, the rate of stress decay during slide-hold simulations is in general agreement with the "Slip law" version of the RSF equations, using parameter values determined independently from velocity step tests. During reslides following long hold times, the model, similar to lab data, produces a nearly constant rate of frictional healing with log hold time, with that rate being in the range of $\sim 0.5 - 1$ times the RSF "state evolution" parameter b. We also find that, as in laboratory experiments, the granular layer undergoes log-time compaction during holds. This is consistent with the traditional understanding of state evolution under the Aging law, even though the associated stress decay is similar to that predicted by the Slip and not the Aging law.

Plain Language Summary

Numerical models of fault slip (earthquakes, earthquake nucleation, landslides, etc.) require "constitutive equations" that describe the time-varying frictional strength of the fault. But despite being studied since Da Vinci, there is no consensus concerning the physics that underlies friction. Laboratory experiments have shown that frictional strength depends upon both the rate of fault slip, and a more nebulous property termed the fault "state". Conventional wisdom is that variations in "state" are generated by time-dependent plastic flow or chemistry at microscopic contact points within the fault. Because faults in the Earth are invariably filled by fragmented rock (gouge), here we explore an alternative model in which variations in friction derive simply from granular rearrangements in a gouge layer, with no rate- or state-dependence at individual grain/grain contacts. Previously, we showed that this model accurately described laboratory experiments in which a gouge layer was subjected to large variations in slip rate. Here we test the same model in "slide-hold-slide" protocols, long used to measure the amount of frictional strengthening that occurs during fault "holds". The study has broad implications for our understanding of the origins of transient friction on faults, an insight needed for improving geological hazard assessment.

1 Introduction

The constitutive framework of Rate- and State-dependent Friction is often used for modeling transient frictional behavior of rocks and other Earth materials (e.g., sediment, glacial till), and for simulating frictional instabilities relevant to earthquakes, landslides and earthflows (J. H. Dieterich, 1992, 1978, 1979; J. H. Dieterich et al., 1981; Ruina, 1983; J. Dieterich, 1994; Marone, 1998; J. H. Dieterich & Kilgore, 1996; Viesca, 2016; Handwerger et al., 2016; McCarthy et al., 2017). A complete prescription of RSF requires an equation for the evolution of the "state variable" defining the "state" of the sliding interface. Existing versions of this equation are largely empirical, differ fundamentally in the extent to which slip or elapsed time is responsible for state evolution, and generally fail to satisfactorily match existing laboratory data beyond the suite of experiments they were designed to describe.

A popular concept has been that in the absence of sliding, state evolution (frictional strengthening, in such cases) is fundamentally a time-dependent process (J. H. Dieterich, 1972). This hypothesis has received support first from the observed logarithmic-with-time growth of contact area between transparent samples of PMMA (Polymethyl methacrylate), due to plastic deformation of contacting asperities (J. H. Dieterich & Kilgore, 1994), and more recently from the logarithmic-with-time increase in acoustic transmissivity across frictional interfaces in rock (Nagata et al., 2012). Log-time frictional strengthening of stationary surfaces has been shown to also result from increased chemical bonding (Li et al., 2011). The log-time increase in both contact area and chemical bonding have been shown to have a sound theoretical basis (Berthoud et al., 1999; Baumberger & Caroli, 2006; Liu & Szlufarska, 2012). Such behavior is embodied in the "Aging" (or "Dieterich") equation for state evolution (Ruina, 1983). Despite its theoretical basis, however, the Aging law accurately describes almost no rock or gouge friction data other than the observed increase in "static" friction with the logarithm of hold time in laboratory slide-hold-slide experiments (as measured by the friction peak upon resliding).

In contrast, a second popular equation for state evolution (the "Slip" or "Ruina" law) has no well-established theoretical justification, but does a remarkably good job describing the results of laboratory velocity-step experiments, as well as the stress decay during the hold portion of slide-hold-slide experiments (Ruina, 1983; Nakatani, 2001; Bhattacharya et al., 2015, 2017). A heuristic explanation for the Slip law was proposed by Sleep (2006), who showed that Slip law behavior can result from a highly nonlinear stress-strain relation at the contacting asperities. The Aging and Slip laws are asymptotically identical for small perturbations from steady-state sliding, but diverge as the sliding deviates further from steady state. Notably, unlike the Aging law, the Slip law predicts no state evolution in the absence of slip. Nonetheless, the Slip law can still generate an increase in frictional strength approximately as log hold time during slide-hold-slide experiments, due to the small amount of slip accompanying the stress decay during holds applied by an elastic testing machine (Ruina, 1983).

The lack of a physics-based theory for transient friction of rock has motivated exploring the physical and chemical origins of rate-state friction in a variety of scientific communities, and has also brought significant attention to the contributions of the quantity (contact area) versus the quality (shear strength) of contact asperities to the state of a frictional interface (Li et al., 2011; Chen & Spiers, 2016; Tian et al., 2017, 2018; Thom et al., 2018). However, future investigations are needed to address the implications of asperity-scale (sometimes single-asperity-scale) observations for the transient frictional behavior at the macroscopic scale. In addition, more work is necessary to determine if any of the single-asperity-scale observations may reproduce or explain the transient frictional behavior of rock and gouge materials in the lab.

In a previous study, we used the discrete element method (DEM) to simulate the transient frictional behavior of a sheared granular gouge layer in a loading configuration that mimicked traditional rock friction experiments (Ferdowsi & Rubin, 2020). We intentionally implemented constant Coulomb friction and no exponential (or thermally activated) creep at grain-grain contacts. We also do not keep track of contact temperatures or include temperature-dependent friction. We then subjected this simulated fault gouge to a series of velocity-stepping protocols. It is noteworthy that most laboratory rock friction experiments become to some extent granular gouge experiments after a short shearing displacement, as a result of wear products that develop on even initially bare rock sliding surfaces, and that the RSF phenomenology is observed in both those experiments that start with bare rock surfaces and those that start with a synthetic gouge layer (Marone, 1998). We found that the sheared granular model, like the Slip law for state evolution, successfully reproduces the characteristic transient frictional response of rock and gouge observed in laboratory velocity-step tests. Furthermore, in that study we investigated a limited number of slide-hold and slide-hold-slide (SHS) tests, and found that the stress decay during the holds were consistent with the predictions of the Slip law, which itself is largely consistent with the stress decay observed in laboratory slide-hold experiments. During the reslides, on the other hand, the simulations deviated from the Slip law prediction, and it did so in a manner that seemed more consistent with laboratory experiments. Together, these results suggested that the granular flow model might do a better job of describing (room temperature, nominally dry) rock and gouge friction experiments than the existing, largely empirical RSF equations. This is surprising. By eliminating time-dependent chemical reactions and plasticity at grain/grain contacts, we are dispensing with what is traditionally considered to be the source of the rate- and state-dependence of rock friction. All the velocity-dependence and transient response of the granular flow model results from momentum transfer between grains, even at our lowest imposed sliding velocities of 10^{-4} m/s. However, it is worth noting that the actual contact stresses in our model, at the default confining pressure of 5 MPa, are ∼1 GPa, large enough that in a physical system exponential creep might be occurring (Berthoud et al., 1999; Baumberger et al., 1999; Rice et al., 2001; Nakatani, 2001). Again, we do not include exponential creep in our model, because our goal is to investigate the extent to which granular rearrangements alone are capable of giving rise to the observed RSF phenomenology.

The purpose of the present paper is to further test the granular flow model as a descriptor of rock friction by more thoroughly examining SHS protocols. Most significantly, we generate a large number of reslides following holds of different durations, to compare the rate of frictional healing in our simulated holds to the logarithmic increase with time seen nearly universally in laboratory data. In addition, for comparison to those data we explore a wider range of system stiffnesses. All the SHS simulations in Ferdowsi and Rubin (2020) were conducted at the highest stiffness we could achieve, that limit being set by the elastic stiffness of the gouge layer itself. For velocity-step tests this is desirable; a high stiffness ensures that the inelastic sliding velocity is always nearly the load point velocity, which allows one to infer the RSF parameters directly from the transient frictional response without having to account for a varying velocity. However, for slide-hold tests the inelastic velocity during the hold is always different from the (zero) load-point velocity, and this velocity is controlled to a large extent by the system stiffness. Because the amount of slip during the load-point hold has been used to help distinguish between the roles of slip and time in frictional healing (Beeler et al., 1994), in this paper we use two additional stiffnesses more appropriate for those laboratory experiments. We also employ a wider range of sliding velocities than in the holds of Ferdowsi and Rubin (2020), as low as 2 mm/s. This is closer to but still somewhat high by laboratory standards. We return to these points in Section 3 of the manuscript.

If, in the face of these more stringent SHS tests, the physics-based granular flow model continues to perform well relative to the the empirical RSF equations, it could help further develop our understanding of the processes underlying rate-state friction. In addition, if by interrogating the model output we are also able to understand the physics underlying the transient response of the model to velocity perturbations, it might allow the development of approximate equations that could be used in numerical simulations of fault slip as a substitute for the RSF equations currently in use. This provides the motivation, in Section 5, for using the SHS simulations to further explore the possibility that the direct velocity-dependence of friction in the granular simulations can be understood in terms of the kinetic energy of the gouge particles (Ferdowsi & Rubin, 2020). We previously found this kinetic energy to be nearly constant for steady-state driving velocities from ∼1 m/s down to the lowest we could achieve, 10^{-4} m/s. The velocities achieved at the ends of our longest load-point holds allow us to extend this observation of near-constant kinetic energy to transient velocities that are 3 orders of magnitude lower still.

We note that even if the granular model performs well relative to the standard RSF equations, this does not imply that time-dependent physical and chemical processes at grain contacts are irrelevant. Indeed, exponential creep is expected at microscopic contacts, and numerous experiments have shown that chemical environment affects the transient behavior of frictional interfaces (Frye & Marone, 2002, e.g.). However, at the moment we lack a physical understanding of state evolution in RSF (in the sense of also being able to match most lab friction data) in any system, experimental or numerical. If we are able to achieve this understanding for the inert granular system, this could shed light on the origins of similar behavior in quite different systems. For this reason the results of this study could be of interest to researchers in the fields of granular physics and glassy systems, as well as, given the ubiquity of granular material in fault zones, researchers in fault mechanics.

This paper is organized as follows: In Section 2, we describe the relevant aspects of rate-state friction, including those aspects that have been seen previously in simulations of granular flow. Section 3 describes the computational model, and important dimensionless parameters that can be used to judge how closely our simulations adhere to the laboratory experiments we compare them to. Section 4 comprises the bulk of the paper - results of the slide-hold and slide-hold-slide simulations and their comparison to relevant lab experiments and models of RSF. Finally, Section 5 looks at the energetics of the slide-hold simulations, with an eye toward further evaluating the idea that the granular kinetic energy can be used to understand the source of the instantaneous velocity-dependence of friction in these simulations.

2 Rate- and State-Dependent Friction background

The empirical framework of rate- and state-dependent friction describes the resistance to sliding as a function two variables: The sliding rate, V, and "something else", commonly referred to as the "state variable" θ, that describes the "state" of the sliding interface. In its simplest form, RSF consists of two equations. The first of these is the "friction equation" alluded to above:

$$\mu = \mu_* + a \log \frac{V}{V_*} + b \log \frac{\theta}{\theta_*} \ . \tag{1}$$

Here μ_* is the nominal steady-state coefficient of friction at the reference velocity V_* and state θ_*. The RSF parameters a and b control the magnitude of velocity- and state-dependence of the frictional strength. The second equation is the "state evolution law" describing the time evolution of the state variable θ. The two commonly used forms are:

$$\text{Aging Law:} \quad \frac{d\theta}{dt} = 1 - \frac{V\theta}{D_c} \tag{2}$$

$$\text{Slip Law:} \quad \frac{d\theta}{dt} = -\frac{V\theta}{D_c} \ln \frac{V\theta}{D_c} \tag{3}$$

where D_c is a characteristic slip distance (J. H. Dieterich, 1979; Ruina, 1983). Eq. 2 is often referred to as the Aging law, as state can evolve with time in the absence of slip; Eq. 3 is often referred to as the Slip law, as state evolves only with slip ($\dot{\theta} = 0$ when $V = 0$). In general, more than one state variable might be required to adequately describe friction as observed in the laboratory (Ruina, 1983; Ikari et al., 2016).

Previous studies have demonstrated that neither the Aging law nor the Slip law adequately describes the full range of laboratory velocity-stepping and slide-hold-slide loading protocols (Beeler et al., 1994; Kato & Tullis, 2001). Velocity-stepping experiments with a sufficiently stiff system show that following a change in velocity, friction approaches its new steady-state value quasi-exponentially over a characteristic slip distance that is independent of both the magnitude and the sign of the velocity step (Ruina, 1983; Marone, 1998; Blanpied et al., 1998; Bhattacharya et al., 2015). This observation holds for both bare rock and gouge samples, and it is consistent with the Slip law prediction for state evolution because the Slip law was designed with that transient behavior in mind (Ruina, 1983; Nakatani, 2001). However, the Aging law predicts a strongly asymmetric and magnitude-dependent transient frictional response to velocity step increases and decreases, behavior that is completely inconsistent with laboratory data (Nakatani, 2001).

The Aging law was introduced primarily to account for the observation that in SHS experiments, beyond a "cut-off time" that is typically of order 1 s, the peak stress upon resliding increases approximately as the logarithm of the hold time (J. H. Dieterich, 1979; J. H. Dieterich & Kilgore, 1994; Marone & Saffer, 2015; Carpenter et al., 2016). However, Bhattacharya et al. (2017) reanalyzed the experimental SHS data of Beeler et al. (1994), conducted using two different machine stiffnesses (and hence two different amounts of interfacial slip during the load-point hold, as the loading machine and rock sample elastically unload), and found that the log-time increase in peak stress upon resliding could be fit about as well by the Slip law as by the Aging law. Bhattacharya et al. (2017) further showed that the nearly logarithmic-with-time stress decay during the load-point holds could be well modeled by the Slip law, which predicts relatively little state evolution owing to the small amount of slip. In contrast, this log-time stress decay is completely inconsistent with the Aging law, which predicts too much strengthening (state evolution) during the holds, and a rate of stress decay that approaches zero as hold time increases (for $a/b < 1$, as was the case in these experiments). Despite the failure of the Aging law to fit both velocity-step tests and slide-hold tests, most theoretical justifications for the evolution of state presuppose mechanisms of time-dependent healing as embodied by the Aging law (e.g., Baumberger et al., 1999). But even the Slip law is unable to model data from both the hold and reslide portions of SHS tests (Bhattacharya et al., 2017).

2.1 Granular rate- and state-dependent friction

Both the empirical nature and the inadequacies of the existing RSF equations motivated our previous study, in which we modeled the behavior of a granular gouge layer with no time-dependent plasticity or chemistry at the grain contacts (Ferdowsi & Rubin, 2020). We subjected the gouge layer to velocity-step numerical protocols over load-point velocities V_{lp} from 10^{-4} to 2 m/s and normal stresses σ_n from 1 to 25 MPa. We found that, in agreement with RSF and multiple previous DEM modeling studies, the simulated granular layer shows a "direct velocity effect" (i.e., an immediate change in friction of the same sign as the imposed velocity step), that is then followed by a gradual "state evolution effect" as friction evolves in the opposite sense toward its new steady-state value (Morgan, 2004; Hatano, 2009; Abe et al., 2002). We further found that the magnitudes of these frictional transients were proportional to the magnitudes of the logarithm of the velocity change, as in RSF, with values of a and b in equation 1 of ~ 0.02, not far from values found in the lab.

We also observed that the granular model appeared be very similar to lab data during slide-hold tests, in that the stress decay during the hold could be well-modeled by the Slip law for state evolution when using parameter values determined independently from velocity-step tests (Bhattacharya et al., 2017, 2021). The results of our preliminary SHS simulations further indicated that the peak stress upon the reslide exceeds the prediction of the Slip law, using the same parameters that fit the hold well. This is similar to behavior observed in lab data (Bhattacharya et al., 2017). Note that some previous studies also either conceptually or qualitatively showed that frictional healing can occur during SHS tests as a result of compaction within the fault gouge (Sleep, 1995, 1997; Nakatani, 1998; Chen et al., 2020). However, as we noted earlier, the simulations of Ferdowsi and Rubin (2020) employed a stiffness that greatly exceeds those that can be achieved in the laboratory. In the current study we also use stiffnesses more similar to laboratory tests.

3 The computational model

We have performed the Discrete Element Method (DEM) simulations reported in this study using the *granular* module of LAMMPS (Large scale Atomic/Molecular Massively Parallel Simulator), a multi-scale computational platform developed and maintained by Sandia National Laboratories (`http://lammps.sandia.gov`) (Plimpton, 1995). The Hertzian potential for grain-grain interaction in this study is realized using the "pair_style gran/hertz/history" in LAMMPS. Our model is made of a packing of 4815 grains, of which there are 4527 in the gouge layer, and 288 in the top and bottom layers (Figure 1). The grains in those top and bottom layers form rigid blocks parallel to the gouge layer and are used to confine and shear the gouge. The grains in the rigid blocks all have a diameter $d = 5$ mm, whereas those in the gouge layer have a polydisperse, Gaussian-like particle size distribution with diameters (d) from 1 to 5 mm, with a mean diameter (D_{mean}) of 3 mm. Grain density and Young's modulus are modeled after glass beads (Table S1). The model domain is rectangular with periodic boundary conditions applied in the x and y directions, with domain size $L_x = L_y = 1.5L_z = 20\ D_{mean}$.

The system is initially prepared by randomly inserting (under gravity) grains in the simulation box with a desired initial packing fraction of ∼0.5. The system is then allowed to relax for about 10^6 time steps, after which it is subjected to confining pressures $\sigma_n = 5$ MPa. The confining pressure is applied for one minute, by which time the fast phase of compaction is completed. The confined gouge sample is then subjected to shearing at a desired driving velocity imposed by a linear spring attached to the top rigid plate, while the vertical position of the top wall is adjusted to maintain a constant confining pressure. The shearing run is continued until the system achieves a quasi-steady state, at which point subsequent loading protocols (slide-holds, slide-hold-slide, velocity step) are imposed on the system.

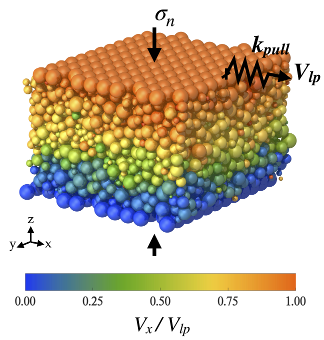

Figure 1. A visualization of the granular gouge simulation. Colors show the velocity of each grain in the x direction, averaged over an upper-plate sliding distance of D_{mean} during steady sliding at a driving velocity of $V_i = 2 \times 10^{-4}$ m/s.

We model grains as compressible elastic spheres that interact with each other when they are in contact via the Hertz-Mindlin model (Johnson, 1987; Landau & Lifshitz, 1959; Mindlin, 1949). The full implementation of the granular physics model used here is described below. The model essentially solves the linear vector equation $F = ma$ for each grain, along with its angular counterpart, with the simplification that the model does not track wave propagation through individual grains. Readers uninterested in the details can skip to the paragraph surrounding equation (12) below.

For two spheres $\{i, j\}$ in contact with each other that have the positions $\{\boldsymbol{r}_i, \boldsymbol{r}_j\}$, and diameters d_i and d_j, the normal ($F_{n_{ij}}$) and tangential ($F_{t_{ij}}$) forces on particle i in its interaction with particle j can be calculated from the following equations:

$$\boldsymbol{F}_{n_{ij}} = \sqrt{\delta}_{ij}\sqrt{\frac{d_i d_j}{2(d_i + d_j)}}(k_n \delta_{ij} \boldsymbol{n}_{ij} - m_{eff}\gamma_n \boldsymbol{v}_{n_{ij}}) \tag{4}$$

$$\boldsymbol{F}_{t_{ij}} = \sqrt{\delta}_{ij}\sqrt{\frac{d_i d_j}{2(d_i + d_j)}}(-k_t \boldsymbol{u}_{t_{ij}} - m_{eff}\gamma_t \boldsymbol{v}_{t_{ij}}) \tag{5}$$

in which k_n and k_t are the normal and tangential stiffness, and are defined as $k_n = (2/3)E/(1-\nu^2)$ and $k_t = 2E/(1+\nu)(2-\nu)$ (Mindlin, 1949). In the relations for the normal and tangential stiffnesses, E and ν are the Young's modulus and Poisson's ratio, respectively, and $m_{eff} = m_i m_j/(m_i + m_j)$ is defined as the effective mass of the two interacting spheres that have masses m_i and m_j. The relative normal and tangential velocities, $\boldsymbol{v}_{n_{ij}}$ and $\boldsymbol{v}_{t_{ij}}$, of the grains used in Eqs. 4 and 5 are defined as:

$$\boldsymbol{v}_{n_{ij}} = (\boldsymbol{v}_{ij} \cdot \boldsymbol{n}_{ij})\boldsymbol{n}_{ij} \tag{6}$$

$$\boldsymbol{v}_{t_{ij}} = \boldsymbol{v}_{ij} - \boldsymbol{v}_{n_{ij}} - \tfrac{1}{2}(\boldsymbol{\omega}_i + \boldsymbol{\omega}_j) \times \boldsymbol{r}_{ij} \tag{7}$$

in which $\{\boldsymbol{v}_i, \boldsymbol{v}_j\}$ are the linear, and $\{\boldsymbol{\omega}_i, \boldsymbol{\omega}_j\}$ are angular components of grain velocities, and $\boldsymbol{r}_{ij} = \boldsymbol{r}_i - \boldsymbol{r}_j$, $\boldsymbol{n}_{ij} = \boldsymbol{r}_{ij}/r_{ij}$, with $r_{ij} = |\boldsymbol{r}_{ij}|$, and $\boldsymbol{v}_{ij} = \boldsymbol{v}_i - \boldsymbol{v}_j$. Additionally, δ_{ij} is the normal compression of the grain and is defined as

$$\delta_{ij} = \tfrac{1}{2}(d_i + d_j) - r_{ij} \tag{8}$$

In Eqs. 4 and 5, the parameters γ_n and γ_t are the normal and tangential damping (viscoelastic) constants of the grain-grain interaction, respectively; For the choices of these two damping constants, we use the default LAMMPS option where $\gamma_t = 0.5\gamma_n$ (it has been shown that the choices of the ratio have little impact on the rheology of granular materials in the dense and quasi-static regime of shearing of hard particles we explore in this work (Ferdowsi & Rubin, 2020; Gaume et al., 2011; da Cruz et al., 2005; Silbert et al., 2001)). In the granular module of LAMMPS, the damping is implemented as a spring and dashpot in parallel for both the normal and tangential contacts.

Having defined the equations for contact forces and torques on each particle, i, we solve the Newton's second law to find the translational and rotational accelerations of particles located in a gravitational field $\boldsymbol{g}$,

$$\boldsymbol{F}_i^{tot} = m_i \boldsymbol{g} + \sum_j \left(\boldsymbol{F}_{n_{ij}} + \boldsymbol{F}_{t_{ij}} \right) \tag{9}$$

$$\boldsymbol{\tau}_i^{tot} = -\frac{1}{2} \sum_j \boldsymbol{F}_{t_{ij}} \times \boldsymbol{r}_{ij} \tag{10}$$

Slip occurs at grain contacts when the local shear stress exceeds the specified (constant) local grain-grain friction coefficient, μ_g. The value of μ_g determines the upper limit of the tangential force between two grains from the Coulomb criterion $F_t \leq \mu_g F_n$. This tangential force grows according to the non-linear Hertz-Mindlin contact law up to the point where $F_t/F_n = \mu_g$. After this point, the tangential force is held at $F_t = \mu_g F_n$ until the point that due to rearrangement of grains either $F_t \leq \mu_g F_n$ or the contact between grains is lost. The rolling friction is set to zero in this study. While the model solves the Newton's second law for each particle, it does not take into account wave propagation inside the grains. In this study, we use a grain-grain friction coefficient of $\mu_g = 0.5$. In Ferdowsi and Rubin (2020) we found that the macroscopic friction, at steady-state and during transients following velocity steps, did not depend strongly on the choice of μ_g in the range $\mu_g = 0.5$ to $\mu_g = 1.0$. In addition, it has been established previously by MiDi (2004) that frictional behavior of sheared granular materials in the dense quasi-static regime of shearing (the regime that we are in) does not depend on the grain-grain friction coefficient (μ_g), as long as μ_g is of order 1 (say larger than 0.1). Please see section 3.4 in MiDi (2004) for further information.

Energy loss at contacts in the granular model is characterized by the "restitution coefficient", which potentially varies from 0 (complete energy loss) to 1 (zero loss). At the low sliding speeds of interest the adopted value of restitution coefficient appears to have very little influence on the macroscopic behavior of the system (Gaume et al., 2011; da Cruz et al., 2005; Silbert et al., 2001). The values of restitution coefficients, ϵ_n and ϵ_t for the normal and tangential directions respectively, are controlled by the choices of the damping coefficients $\gamma_{n,t}$ and contact stiffness $k_{n,t}$. For the Hertzian grain contact law, the restitution coefficient in the normal direction is obtained from the equation of relative motion of two spheres in contact:

$$\ddot{\delta} + \frac{E\sqrt{2d_{eff}}}{3m_{eff}(1-\nu^2)} \left(\delta^{3/2} + \frac{3}{2} A \sqrt{\delta} \dot{\delta} \right) = 0 \tag{11}$$

with the the initial condition $\dot{\delta}(0) = \boldsymbol{v}_n$ and $\delta(0) = 0$. The variable A is defined as $A = \frac{1}{3} \frac{(3\gamma_t - \gamma_n)^2}{(3\gamma_t + 2\gamma_n)} \left(\frac{(1-\nu^2)(1-2\nu)}{E\nu^2} \right)$, and $d_{eff} = d_i d_j/(d_i + d_j)$ is the effective diameter for spheres of diameters d_i and d_j. From solving this equation, the normal component of the coefficient of restitution is defined as the ratio of normal velocity of grains at the end of the collision, defined as $\dot{\delta}(t_{col})$, to the initial normal impact velocity of the grains: $\epsilon_n = \dot{\delta}(t_{col})/\dot{\delta}(0)$. Solving the same equation also gives the collision time t_{col} for given choices of the physical properties of grains and the initial velocity with which two grains collide. The restitution coefficient in the tangential direction can be obtained from a similar procedure but with implementing a tangential damping coefficient (Brilliantov et al., 1996). The time step of our simulations is defined as $\Delta t = t_{col}/100$, with t_{col} evaluated here with the assumption of an impact velocity $\dot{\delta}(0)$ of 25 m/s (to be on the safe side for the choice of the simulation time-step and to solve the equations of motions accurately; grain-grain impact velocities are highly unlikely to achieve 25 m/s in the quasi-static simulations reported in this work). The time-step $\Delta t = t_{col}/50$ is based on previous values used and is recommended by Silbert et al. (2001). The majority of the simulations in this study were performed with a very high restitution coefficient of $\epsilon_n = 0.98$, corresponding roughly to performing experiments on gouge saturated with dry air. However, we also have run a series of slide-hold simulations with a much lower restitution coefficient of $\epsilon_n = 0.3$. Consistent with previous DEM studies at low sliding speeds, we find that the adopted value of the restitution coefficient appears to have very little influence on the macroscopic behavior of systems in the dense granular flow regime (Gaume et al., 2011; da Cruz et al., 2005; Silbert et al., 2001; Ferdowsi & Rubin, 2020) (see also Figure 9 of this paper). The full details of the granular module of LAMMPS are described in the LAMMPS manual and several references (Zhang & Makse, 2005; Silbert et al., 2001; Brilliantov et al., 1996). Unless otherwise specified in this paper, all details of the present model, except for the values of pulling spring stiffness, are identical to the "default" model of Ferdowsi and Rubin (2020). Standard values of some of the adopted parameters are listed in Table 1.

Table 1. DEM simulation parameters. If in some limited simulations, different parameter values are used, they are explicitly mentioned in the text.

Parameter	Value
Grain density, ρ	2500 [kg/m^3]
Young's modulus, E	50 [GPa]
Poisson ratio, ν	0.3
Grain-grain friction coefficient, μ_g	0.5
Confining pressure, σ_n	5 [MPa]
Coefficient of restitution, ϵ_n	0.98
Time step, Δt	2×10^{-8} [s]

The relation of the velocity V in equations (1)–(3) to the granular simulations merits some discussion. In particular, this V is not the velocity of the upper (driving) plate. In laboratory experiments, slip parallel to the frictional interface is monitored between two points on opposite sides of, and some distance from, that interface, and the actual (inelastic) slip δ is estimated from

$$\begin{aligned} \delta &= \delta_{lp} - \delta_{el} = \delta_{lp} - \tau/k \; ; \\ \tau &= k(\delta_{lp} - \delta) \, . \end{aligned} \tag{12}$$

Here δ_{lp} is the measured "load-point" displacement, δ_{el} is the elastic distortion of the system between the monitoring points resulting from stress changes, τ is the measured stress, and k is the elastic stiffness of the combined testing apparatus plus sample between the monitoring points (units of stress/distance). Taking the time-derivative of (12) leads to an estimate of the sliding speed as a function of measured quantities. Conceptually, δ in lab experiments is often treated as occurring on a discrete plane, but, just as in our numerical simulations, it actually occurs over a region whose thickness is a priori unknown.

We treat our model output in the same way. δ_{lp} is the displacement of the end of the spring at which the velocity is imposed, and τ is the spring force divided by the 6 cm × 6 cm surface area of the driving plate. The effective stiffness k is given by treating the spring and gouge as being in series:

$$k = \frac{k_{sp} k_H}{k_{sp} + k_H} \tag{13}$$

where k_{sp} and k_H are the spring and gouge stiffness, respectively, and H denotes the gouge thickness. Equivalently, we could treat the "load-point" displacement δ_{lp} as being the measured displacement of the driving plate, in which case $k = k_H$ (showing, after insertion into (12) and differentiating, that V is not the velocity of the upper plate if the stress is changing, as this changes the elastic distortion of the gouge).

The shear modulus of the gouge layer can be estimated from the initially linear (nearly elastic) portion of the loading stress-strain curve at the start of a steady-sliding test. In Fig. B1 of Ferdowsi and Rubin (2020), we show the sensitivity of the gouge shear modulus to hold time duration in SHS tests, and we find that at 5 MPa $G_H \approx 270 - 310$ MPa regardless of hold time. From the value of shear modulus $G_H \approx 300$ MPa, the stiffness k_H can be determined as $k_H = G_H/H = 7.3 \times 10^9$ Pa/m, where $H = 0.04$ m is the gouge thickness. We can further determine k_{sp} in Pa/m from the spring stiffness input, k_{pull}, in LAMMPS in units of N/m, by dividing k_{pull} by the sample surface area. We use 3 pulling spring stiffnesses: $k_{pull} = 1 \times 10^{10}, 8 \times 10^5,\; 2.7 \times 10^4$ N/m corresponding to dimensionless system stiffness $\bar{k}_d \equiv kD_c/(b\sigma) \approx 425,\; 12,\; 0.4$, respectively, where the "≈" sign indicates that the values of the normalizing constants b and D_c, determined from fitting simulated velocity-step tests, are known only to within about 10%. The dimensionless stiffness $\bar{k}_d \approx 425$ represents the approximate upper bound for what we can achieve; $k_{pull} = 10^{10}$ N/m is large enough that essentially all the elastic compliance comes from the gouge. The dimensionless system stiffnesses of $\bar{k}_d \approx 12$ and 0.4 were chosen to be close to the values of $\bar{k}$ in the SHS experiments performed on the rotary shear apparatus of Beeler et al. (1994), to which we compare some of our granular model observations. After performing the granular simulations reported in this work, our estimates of $\bar{k}_d$ for those lab data, based on the analysis of Bhattacharya et al. (2021), were reduced by 1/3 from their initial values, to $\bar{k}_d \approx 8$ and 0.27, so the match with our simulations is not exact. For analysis of our simulation data we used values of $D_c = 1.77 D_{mean} = 0.0053$ m, $a = 0.0247$, and $b = 0.0178$ which were obtained from velocity-stepping simulations (Ferdowsi & Rubin, 2020).

Unlike most laboratory experiments on gouge, we do not see strain localization within our system. We do not consider grain breakage, a process which may contribute to localization in the lab and in DEM simulations (Abe & Mair, 2009). Our gouge layer is also only about 14 median grain diameters thick, which may be too narrow for localization, although in our previous work, we did not observe localization in simulated gouge layers that were either ∼14 or 25 grains thick. Experimental studies summarized by Rice (2006) suggested that shear bands in granular sands satisfy the condition $D_{mean}/H_{eff} \sim 1/10 - 1/20$ for the ratio of mean grain diameter to active thickness of the gouge layer. However, it is not clear that localization should be expected in a gouge layer that, as in our simulations, strengthens as the shearing rate increases. Previous studies on fault zone rheology suggest that strain-rate-weakening is a necessary condition for localization in sheared fault gouge (Tse & Rice, 1986; Sleep, 1997; Rice & Cocco, 2007).

Friction in our simulations is defined as the ratio of the shear to normal force exerted on the upper rigid block by the gouge grains in contact with it. If accelerations of the upper plate are unimportant, this shear force can be equated with the force applied by the pulling spring in (12). If the plate velocity suddenly changes to or from ∼1 m/s, this assumption is violated and wave propagation within the gouge must be considered (Ferdowsi & Rubin, 2020, Appendix B). The SHS simulations reported here were run with initial steady-state velocities of $V_i = V_{lp} = 2 \times 10^{-3}$, 2×10^{-2}, and 10^{-1} m/s, and in most simulations we used a reslide velocity equal to the initial velocity. However, in a small number of cases we changed the reslide velocity to search for deviations from the predictions of existing RSF equations; any such deviations would be relevant to models of earthquake nucleation. We also performed a series of slide-hold simulations at the smaller initial sliding velocity of $V_i = 2 \times 10^{-4}$ m/s. In laboratory experiments, the sliding velocity is typically on the order of $1 - 10$ μm/s; however, running simulations at such velocities is not yet possible with the DEM method within reasonable computational costs, provided one uses grain elastic properties and densities appropriate for quartz-like materials. Our fully parallelized simulations at sliding velocities of $V_i = 2 \times 10^{-2}$, 2×10^{-3} and 2×10^{-4} m/s, took about a few days, two weeks, and six weeks of real time, respectively, to achieve steady-state friction on Princeton's PICSciE's computational cluster. The longest holds took 5 months.

To assess the importance of our deviation from lab-like parameters, we turn to dimensionless ratios. The sliding velocity enters only one – the Inertial number, a critical parameter in granular flows, defined as $I_n \equiv \dot{\gamma} D_{mean} \sqrt{\rho/P} \approx V(D_{mean}/H)\sqrt{\rho/P}$, where $\dot{\gamma}$ is the local shear rate, the approximate equality is appropriate for our loading geometry, P is the confining pressure (synonymous with the normal stress in these simulations), and ρ and D_{mean} are the density and mean diameter of grains, respectively. The inertial number measures the ratio of the inertial forces of grains to the confining forces acting on those grains, such that small values ($I_n \lessapprox 10^{-3}$) correspond to the dense, quasi-static regime of shearing that we desire to model (da Cruz et al., 2005; Forterre & Pouliquen, 2008). The SHS simulations reported here with $V_i = 2 \times 10^{-3}$ to 10^{-1} m/s have inertial numbers during steady sliding satisfying $\sim 10^{-6} \lesssim I_n \lesssim 10^{-4}$, all in this quasi-static regime. Ferdowsi and Rubin (2020) explore the range $\sim 10^{-7} \lesssim I_n \lesssim 10^{-3}$ during velocity-step tests, and find no significant variation in the RSF parameter values. There is no a priori expectation that the RSF parameters will begin to vary at still lower I_n, but of course one does not know this, and testing for systematic changes with V_i provides the motivation for performing SHS tests at a range of achievable sliding velocities within the quasi-static regime.

Confining pressure enters the Inertial number discussed above as $P^{-1/2}$, and also the "dimensionless pressure" $\bar{P} = (P/E)^{2/3}$, where E is Young's modulus (50 GPa in our simulations). $\bar{P}$ is a measure of the grain strain at the imposed confining pressure; the 2/3 power is appropriate for contacting elastic spheres (Hertzian contacts). With $P = 5$ MPa, $\bar{P} = 2 \times 10^{-3}$ in our simulations. Ferdowsi and Rubin (2020) explored values $0.7 \times 10^{-3} \lesssim \bar{P} \lesssim 6 \times 10^{-3}$ ($1 < P < 25$ MPa), and found only modest variations in the RSF parameter values. Rather than tailor our values of $\bar{P}$ to individual experiments, we chose to maintain the default value of $P = 5$ MPa in Ferdowsi and Rubin (2020), and rely on their observation that the RSF parameters do not seem to be very sensitive to this choice.

In contrast, there is reason to believe that the choice of system stiffness in our slide-hold and SHS simulations is quite important. For the longest (load-point) holds conducted by Beeler et al. (1994), one can estimate (from their reported stress drops and stiffnesses) that there was $\sim$2.4 μm of accumulated slip in their high-stiffness case and $\sim$16 μm of slip in their low-stiffness case. For $D_c \sim 2\mu$m (Bhattacharya et al., 2021) this corresponds to roughly $1.2D_c$ and $8D_c$ of slip. Given the potential importance of slip on the order of D_c to state evolution, this difference is quite significant. For a complete list and discussion of the governing dimensionless variables of the model, see Appendix A of Ferdowsi and Rubin (2020). As one last point, we note that reducing all length scales (the grain size and all model dimensions) by the same factor, while keeping V_i the same, results in simulations that are dimensionally identical.

4 Results and discussion

4.1 General considerations

Before proceeding to the results of the granular simulations, it is worth considering what it means to "compare" our results to laboratory experiments. The ratio a/b for the granular simulations, determined from simulated velocity steps, is $\sim$1.4, and may be fixed by our choice of spherical particles, Gaussian-like grain size distribution, and the tangential and normal contact laws we have adopted (for example, Ferdowsi and Rubin (2020) found that a more exponential-like grain size distribution gave rise to simulations with values of a/b much closer to 1; we did not pursue those here because they were noisier and would have required even larger system sizes and more computational resources to see clear signals). The value $a/b \sim 1.4$ is slightly high by lab standards, and we are not aware of lab experiments that push surfaces with such values far enough from steady state to be useful for constraining models of state evolution. Therefore we do not necessarily expect our granular simulations to match any particular lab experiment. Nonetheless, we were able to claim that the simulations successfully capture the phenomenology of laboratory velocity-step experiments. This phenomenology entails that the amplitudes of the changes in friction with velocity and state are proportional to the logarithm of the velocity step (amplitudes controlled in RSF by the parameters a and b), and that friction evolves to its future steady state value over a characteristic slip distance (D_c), independent of the size or sign of the velocity step. Because, by design, these attributes of lab experiments are replicated by the Slip version of the RSF equations, it was convenient to use Slip law fits to our simulation output to determine the values of a, b, and D_c that fit our data well (note that absent some conceptual model for friction, we could not even have made the statement above that in our simulations "$a/b \sim 1.4$").

For slide-hold tests the situation is more complicated, because it is less obvious what the "phenonomenology" of laboratory holds is. Here we made more essential use of comparisons between our simulations and the predictions of the Aging and Slip laws for state evolution, on the one hand, and comparisons between the Aging and Slip laws and laboratory experiments, on the other. Bhattacharya et al. (2017; 2021) showed that the stress decay during laboratory holds was fit reasonably well by Slip law simulations, using parameter values determined independently from velocity steps, and that the Aging law, with its time-dependent healing, predicted too little stress decay. Because these features of the lab data were replicated by our numerical simulations, we used this indirect comparison (granular simulations to RSF / RSF to lab data) to claim that the granular simulations also seemed to do a good job matching laboratory slide-hold experiments (although, as we noted previously, the comparison in Ferdowsi and Rubin (2020) was made using a system stiffness that exceeds those achievable in the lab). For SHS tests, the salient phenomenology is that the peak friction upon resliding increases nearly linearly with the logarithm of hold time. For the Aging law, which was designed to produce this behavior, the slope of this increase (suitably normalized, i.e., converting between the base 10 and natural logarithms) is the RSF parameter b, whereas in lab experiments it seems to be variable but roughly a factor of 2 smaller (see Section 4.3). So although in this case we could "compare" the slope in our simulations directly to lab data without seeming to reference the Aging law, in fact by choosing to compare the slope to b we are implicitly making use of the Aging law. That is, absent some moderately successful model prediction, it is not apparent what we should be comparing the slope of our healing relation to.

4.2 Slide-hold simulations

In this section we present the slide-hold (SH) behavior of the granular model. Since individual simulations tend to be somewhat noisy, all simulation signals presented in this manuscript are averaged over eight different realizations (initial grain arrangements) of the model, all subjected to the same boundary conditions. Friction is defined as the ratio of shear to normal stress τ/σ, where τ is the shear force per unit area exerted by the gouge particles on the upper (driving) plate, and σ is the normal force per unit area on the upper plate.

Figures 2a-c show the variation of normalized friction with normalized hold time for SH tests, with initial sliding velocities of $V_i = 2 \times 10^{-3}$, 2×10^{-2}, and 10^{-1} m/s shown by the cyan, blue, and black curves, respectively. Panel (a) shows the results of simulations run with system stiffnesses $\bar{k}_d \approx 425$, while panels (b) and (c) show simulations with system stiffness $\bar{k}_d \approx 12$ and $k_d \approx 0.4$, respectively. Based on the indicated reductions in friction and the system stiffnesses, the longest holds in these simulations correspond to total (inelastic) slips within the gouge layer of roughly (from most to least stiff) $0.04D_c$, D_c, and $10D_c$.

Lowering the stiffness delays the onset of stress decay because a given stress reduction then requires a longer slip distance; at constant sliding velocity, elasticity dictates that the normalized friction change $\Delta\mu/b$ reaches -1 when $t_{hold}/(D_c/V_i) = \bar{k}^{-1}$, which is roughly when the stress trajectories in Figure 2 leave their initial plateau (the Slip law predictions for $\bar{k}_d \approx 12$ and $\bar{k}_d \approx 0.4$ have been included in panel (a) for reference). From dimensional analysis, standard RSF (equations 1–3 with constant parameter values) predicts that the curves for the same $\bar{k}$ but different V_i overlap identically when plotted versus dimensionless hold time $\bar{t}_{hold} \equiv t_{hold}/(D_c/V_i)$. Our simulations at the three sliding velocities with $\bar{k}_d \approx 425$ show a stress decay response that is not exactly the same, but they are nevertheless similar to each other within their standard deviations. The stress decay response for the three velocities differ more significantly at the lower (lab-like) stiffnesses of $\bar{k}_d \approx 0.4$ and 12. Existing lab data addressing this question are mixed. The slide-hold experiments of Marone and Saffer (2015) using simulated gouge show a modest dependence on V_i, when plotted vs. normalized hold time, but those of Bhattacharya et al. (2021) on initially bare rock surfaces that develop a gouge layer do not.

Figures 2a-c also include the predictions of the Aging and Slip laws for the stiffnesses used in the granular model. These predictions are obtained using the RSF parameter values determined independently from Slip law fits to simulated velocity steps performed on the identical granular system (Ferdowsi & Rubin, 2020). We do not use parameter values determined using the Aging law because that model is clearly inappropriate for modeling velocity steps, in both laboratory experiments and our DEM, as the Aging-law estimate of D_c depends entirely upon the magnitudes and signs of the velocity steps one chooses to fit (Bhattacharya et al., 2015) (for stiff systems, such as that used by Ferdowsi and Rubin (2020), only the value of D_c, and not a and b, depend upon the adopted state evolution law). For $\bar{k}_d \approx 425$, the stress decay of the granular model is in excellent agreement with the Slip law prediction. There is also reasonable agreement for the lower stiffnesses of $\bar{k}_d \approx 0.4$ and 12, where the Slip law prediction generally lies between the curves for the different V_i (we return to the differences between the different V_i below). In contrast, for the two larger stiffnesses, where the Aging- and Slip-law predictions differ, the Aging-law significantly underestimates the stress decay at long hold times. The shallowing slope of the stress decay for the Aging law results from its pre-

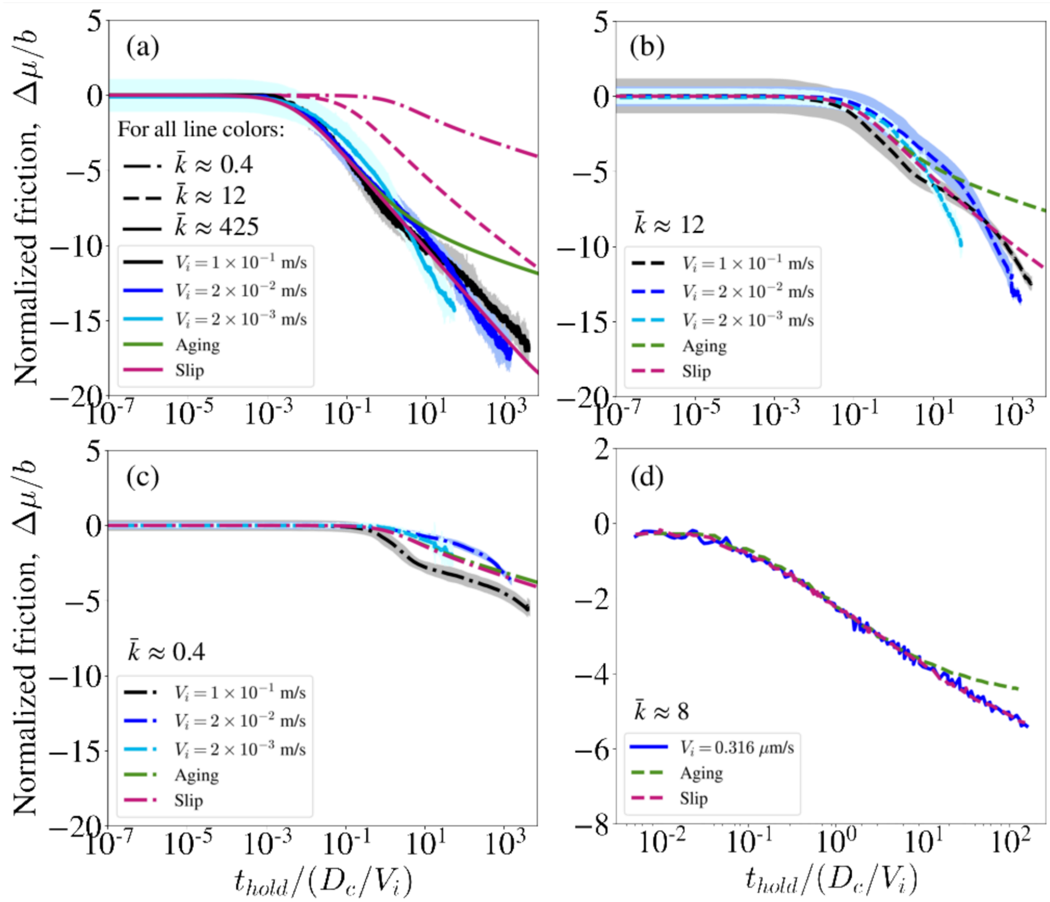

Figure 2. The slide-hold behavior: The cyan, blue, and black lines in panels (a-c) show the variation of friction coefficient, normalized by the RSF parameter b, as a function of normalized hold time, for granular slide-hold simulations with prior sliding velocities V_i of 2×10^{-3} (cyan), 2×10^{-2} (blue), 10^{-1} (black) m/s. Panels (a), (b), and (c) show the behavior of the systems with stiffness $\bar{k}_d \approx 425$, 12, and 0.4, respectively. The pink and green lines in panels (a-c) further show the predictions of the Slip and Aging laws, respectively, using the RSF parameters ($D_c = 0.0053$ m, $a = 0.0247$, $b = 0.0178$) determined independently from Slip-law fits to velocity-step tests performed on the same model (Ferdowsi & Rubin, 2020). The predictions of the Slip and Aging laws are shown with different line styles for different system stiffnesses (the Slip law predictions for $\bar{k} = 12$ and 0.4 are included in panel (a) only for reference). Granular simulation results in panels (a-c) are averaged over 8 different realizations (initial grain arrangements) subjected to the same imposed loading conditions. Black, blue, and cyan lines show the mean behavior of the realizations for each system, and the width of the gray, blue, and cyan shades around each line shows the 2-sigma deviations. The confining pressure in all simulations is 5 MPa. (d) The blue line shows the variation of friction coefficient, normalized by the RSF parameter b, as a function of normalized hold time, for an experiment performed in the Tullis rotary shear apparatus at Brown University on a granite sample with prior sliding velocity $V_i = 0.316\ \mu$m/s. The system stiffness for this experiment is $\bar{k}_d \approx 8$, and the confining stress is 25 MPa. As in panels (a-c), the pink and green lines show predictions of the Slip and Aging laws, respectively, using the RSF parameters ($D_c = 2\ \mu$m, $a = 0.013$, $b = 0.016$) obtained from Slip-law fits to velocity-step tests on the same experimental sample. We used the same RSF parameters to calculate the dimensionless stiffness $\bar{k}$ for the lab data.

diction of continual state evolution, $\dot{\theta} \approx 1$ in equation 2, even at vanishing slip rates. Analytically, the slope of the stress decay at long hold times for the Aging law (with $a/b > 1$) is $(1 - a/b)$ when plotted vs. $\ln(\bar{t}_{hold})$, and $2.3(1 - a/b)$ when plotted vs. $\log_{10}(\bar{t}_{hold})$, independent of the system stiffness (Bhattacharya et al., 2017, Appendix C). For the Slip law, the long-time slope in general depends upon stiffness, but in the "infinite-stiffness limit" it is $2.3(-a/b)$ when when plotted vs. $\log_{10}(\bar{t}_{hold})$ (Bhattacharya et al., 2017), which for the parameter values of our granular simulations is 3.6 times larger. All 3 initial velocities for $\bar{k} \approx 425$ in Figure 2a, and the corresponding Slip-law prediction, have this "infinite-stiffness limit" slope. For $\bar{k}_d = 0.4$ in Figure 2c, there is sufficiently little reduction in slip speed that the predictions of the Aging and Slip laws are extremely similar.

Because our initial sliding velocities are higher than those typically used in laboratory slide-hold experiments, it is important to assess any systematic trends with V_i in the granular simulations. At the highest stiffness ($\bar{k} \approx 425$), the curves for the different V_i tend to weave around the Slip-law prediction, but they all end up with the same (Slip-law) slope at the longest hold times. At short hold times for $\bar{k} \approx 12$ and 0.4, there do not seem to be trends that are monotonic with V_i, with the slowest velocity (2×10^{-3} m/s) plotting between the two larger velocities. However, at the longest hold times in Figure 2b ($\bar{k} \approx 12$), there is a systematic trend of lower stress with lower V_i. Whether this trend would persist to longer hold times is not known.

An example of frictional behavior during a laboratory slide-hold experiment on rock is shown in Fig. 2d, from Bhattacharya et al. (2021). The experiment was performed on a granite sample with initial sliding velocity $V_i = 0.316$ μm/s, system stiffness $\bar{k}_d \approx 8$, and confining stress 25 MPa. The Aging and Slip law predictions for the experiment are shown with green and pink lines, respectively. These predictions, similar to the RSF predictions for the granular model, are obtained using the RSF parameter values determined independently from Slip law fits to velocity-stepping experiments on the same sample. Overall, as with the fits to the granular simulations, they indicate that the Aging law underestimates the stress decay in the lab at long hold times, while the Slip law provides a very good prediction of the behavior. Comparing the behavior of both the lab data and the granular model to the Aging and Slip law predictions, especially Figures 2b and 2d with close to the same stiffness, we conclude that although the stress decay in the simulations is not strictly log-linear as for the lab data, the granular model qualitatively captures the stress decay observed in laboratory slide-hold tests.

The stress decay during slide-hold protocols clearly rules out the Aging law for the evolution of state in both the granular model and laboratory experiments. This is despite the fact that log-time fault-normal compaction is almost universally observed during laboratory holds under room-humidity conditions. This compaction is thought to be consistent with an Aging law-like evolution of state; that is, in theoretical justifications of the Aging law, the same mushrooming of highly-stressed contacts that is considered to be responsible for log-time increase of true contact area and frictional strength, would also lead to log-time compaction (Berthoud et al., 1999; Sleep, 2006). The same argument would suggest that if the stress data during holds is well modeled by the Slip law, with its relative lack of state evolution, the fault-normal compaction would be much less. This potential conflict between the stress and fault-normal displacement data from laboratory holds was noted previously by Bhattacharya et al. (2017).

In our previous work, we observed that in addition to matching the stress decay during laboratory holds, the granular model led to log-time reduction in gouge thickness for $\bar{k}_d \approx 425$ (Ferdowsi & Rubin, 2020). Here we examine the changes in gouge thickness during slide-holds using stiffnesses more appropriate for lab experiments. Figure 3a shows the gouge compaction with hold time in the granular model with stiffnesses $\bar{k}_d \approx 425$ and 12, in comparison to the gouge compaction observed in the laboratory for two system stiffnesses $\bar{k}_d \approx 8$ (filled circles) and 0.27 (lab data from Beeler et al. (1994), as reported by Bhattacharya et al. (2017)). The lab experiments were performed in a rotary shear apparatus, so there is no need to correct for sample dilation/compaction due to a Poisson effect as the loading stress changes (Beeler et al., 1996). The gouge compaction in the granular model with the lower stiffness $\bar{k}_d \approx 0.4$ is shown separately in Fig. 3b for clarity, where now the lab data for $\bar{k}_d \approx 0.4$ are shown as filled circles. These plots indicate that the magnitude of gouge compaction in the granular model is in general agreement with laboratory observations,

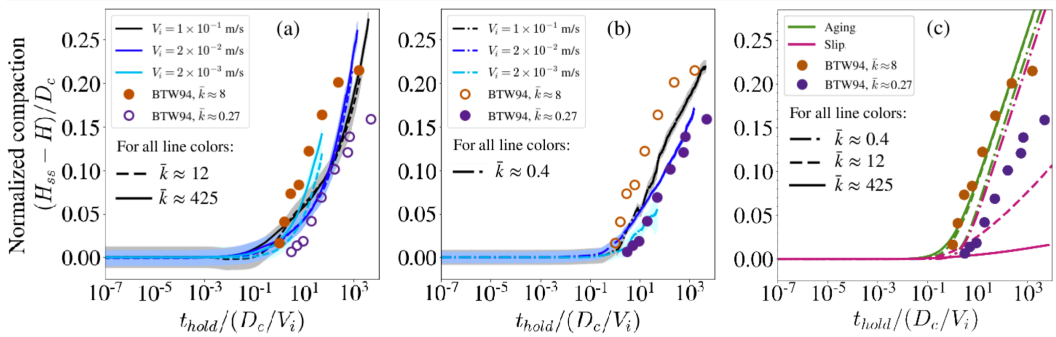

Figure 3. Gouge compaction during slide-holds: The cyan, blue, and black lines in panels (a) & (b) show the variation of gouge compaction, normalized by the RSF characteristic slip distance D_c, as a function of normalized hold time, for granular slide-hold simulations with prior driving velocities V_i of 2×10^{-3} (cyan), 2×10^{-2} (blue), and 10^{-1} (black) m/s. Panel (a) shows the behavior for stiffnesses $\bar{k}_d \approx 425$ and 12, while panel (b) shows the behavior of stiffness $\bar{k}_d \approx 0.4$. The widths of the gray, blue, and cyan shades around the mean behavior lines indicate 2-sigma deviations. (c) The pink and green lines show the evolution of log(state) under the Slip and Aging laws, respectively, using the RSF parameters determined independently from Slip-law fits to velocity-step simulations (Ferdowsi & Rubin, 2020). The state evolutions are scaled by the factor $-d(H_{ss}/D_c)/d\log\theta \approx 0.035$ (Fig. 2c in Ferdowsi and Rubin (2020)), where the H_{ss} is the steady-state thickness of the granular layer (see text for discussion). Different line styles correspond to different system stiffnesses as described in the legend. The filled and empty dots in all panels show the change in gouge thickness during hold experiments on a granite sample reported by Beeler et al. (1994), who used two different ($\bar{k}_d \approx 8$ and 0.27) machine stiffnesses. The dots are filled or empty in panels (a) and (b) depending on the machine stiffness that is most appropriate to compare the granular model behavior to in that panel. An estimated slip-weakening distance $D_c \approx 2\mu$m is used to normalize compaction data in laboratory experiments (Bhattacharya et al., 2021). The lab experiments with stiffness $\bar{k}_d \approx 0.27$ and 8 were performed with sliding velocities $V_i = 1$ μm/s and 0.32 μm/s, respectively. Both low and high stiffness laboratory experiments were performed at 25 MPa confining pressure.

after both are normalized by their appropriate value of D_c. For the granular simulations this is the sensible normalization; Ferdowsi and Rubin (2020) found that the ratio of gouge thickness changes to D_c was independent of the nominal gouge thickness over the range they explored. For the lab data, normalization by D_c is intended to account for the fact that deformation is typically localized over a layer of unknown thickness; inherent in this approach is the assumption that both slip and compaction are concentrated within this layer. Together, panels (a) and (b) show that gouge compaction in the granular model is much less strongly dependent on system stiffness than is the stress decay, and that the normalized rate of compaction with log time is close to that of the lab data (most obviously for the simulation with lowest stiffness, panel (b), which is also the simulation for which the compaction is most nearly log-linear). The lab data show more of a stiffness-dependent offset along the time axis than do the simulations, although the simulations with the lowest V_i of 2×10^{-3} m/s show a modest offset of the proper sign.

The relatively weak dependence of the compaction rate on stiffness in the granular simulations is reminiscent of the Aging-law prediction for the evolution of state θ, because for long Aging-law holds $\dot{\theta} \sim 1$, independent of all else. Fig. 3c shows the evolution of log(state) as predicted using the RSF Aging and Slip laws (in green and red, respectively), for the three stiffnesses used in the granular model. To plot log(state) on the same axis as compaction, we use the linear relation between steady-state gouge thickness and log velocity found by Ferdowsi and Rubin (2020), combined with the RSF relation that at steady state velocity is inversely proportional to state. That is, we multiply the computed change in log(state) by the factor $-d(H_{ss}/D_c)/d\log\theta$, found to be ~0.035 in Figure 2c of their paper, where H_{ss} is the steady-state thickness of the gouge layer. The agreement between this Aging law prediction and the lab data, and from comparison to Figures 3a and 3b the agreement between the granular simulations and the lab data, is quite remarkable. The evolution of state under the Slip law for the lowest stiffness is, as with the stress decay, very similar to that for the Aging law. However, as the system stiffness increases, the evolution of state under the Slip law significantly decreases because the amount of slip decreases. Translating this state evolution to fault-normal compaction as in Figure 3c, the prediction would be that compaction for the Slip law should be strongly stiffness-dependent, completely unlike compaction in the simulations and in the lab data. All of this serves to emphasize the point that while stress during the holds is fit well by the Slip law, compaction during the holds is fit much better by the Aging law prediction of state evolution.

4.3 Slide-hold-reslide simulations

A main motivation for conducting SHS experiments on rock is to better understand the fault healing that occurs during interseismic intervals, healing that is necessary for repeated earthquakes to occur on the same section of fault. This healing historically has been measured by the peak stress $\Delta\mu_{peak}$ upon resliding following a hold (see the inset in Figure 4a), under the assumption that little state evolution occurs in the short time or slip distance between the start of the reslide and the peak stress (we leave aside here the question of whether room temperature and humidity experiments are relevant to natural faults at depth). Because the Aging law embodies fault healing (state evolution) with time even in the absence of slip, for the same parameter values it generates more healing during holds than the Slip law. More diagnostically, sufficiently long hold times lead to $V\theta/D_c \ll 1$, so from equation 2 for the Aging law, $\dot{\theta} \approx 1$. This means that for long hold times the rate of healing with log hold time is independent of how much slip accumulates during the hold, and hence it is independent of the elastic stiffness of the loading system (Beeler et al., 1994; Bhattacharya et al., 2017). These authors further showed that the Aging law predicts that the reduction in log(state) between the start of the reslide and peak stress is independent of hold duration, and hence that the predicted change in peak friction with log hold time, $d\Delta\mu_{peak}/d\ln(\bar{t}_{hold})$, equals the RSF parameter b (equation (1); note that at peak stress $d\tau/dt = 0$, so from elasticity the sliding velocity at5 that moment equals the load-point velocity). This property was exploited by Beeler et al. (1994), who ran lab experiments with two loading machine stiffnesses and found that, indeed, for long hold times, the rate of healing was independent of stiffness. Bhattacharya et al. (2017) later showed that, for the two stiffnesses and hold durations of those experiments, the same stiffness-independent rate of healing could be achieved by the Slip law, but over a more restricted range of RSF parameters. Those parameters do not include the ratio of a/b appropriate for our granular simulations.

It is well established from decades of laboratory experiments on rock and gouge that the peak friction upon resliding increases nearly linearly with log hold time (J. H. Dieterich, 1972; Beeler et al., 1994; Baumberger & Caroli, 2006; Marone & Saffer, 2015; Carpenter et al., 2016). The only study of which we are aware that compares the observed rate of increase to the Aging law prediction, $d\Delta\mu_{peak}/d\ln(\bar{t}_{hold}) = b$, using values of b determined independently from velocity-step tests, is the combined work of Ikari et al. (2016) and Carpenter et al. (2016) on natural and synthetic gouge materials. Excluding their synthetic clay gouges, for which our granular simulations with spherical grains are likely inappropriate, Ikari et al. (2016) found slopes mostly in the range of $\sim 0.3b$ to $0.7b$. Beeler et al. (1994) found $d\Delta\mu_{peak}/d\ln(\bar{t}_{hold}) \sim 0.01$ for their granite sample, close to the expected value of b for granite, but a slope of ~0.004 for quartzite, probably a factor of ~2 lower than the expectation for b. Marone and Saffer (2015) found slopes of ~0.0035, plus or minus several tens of percent depending upon V_i, values that seem within the range of Ikari et al. (2016).

Beyond this, results seem to be limited to single studies. As mentioned previously, Beeler et al. (1994) showed that the rate of frictional strengthening $d\Delta\mu_p/d\ln(\bar{t}_{hold})$ was independent of system stiffness, and interpreted this as suggesting that frictional healing depends upon time rather than slip. Marone and Saffer (2015) showed that the rate of frictional strengthening in their synthetic gouge samples depended upon V_i, increasing by nearly a factor of 2 over the range 1–100 μm/s, indicative of a velocity-dependence of the RSF parameters or a characteristic velocity in the governing

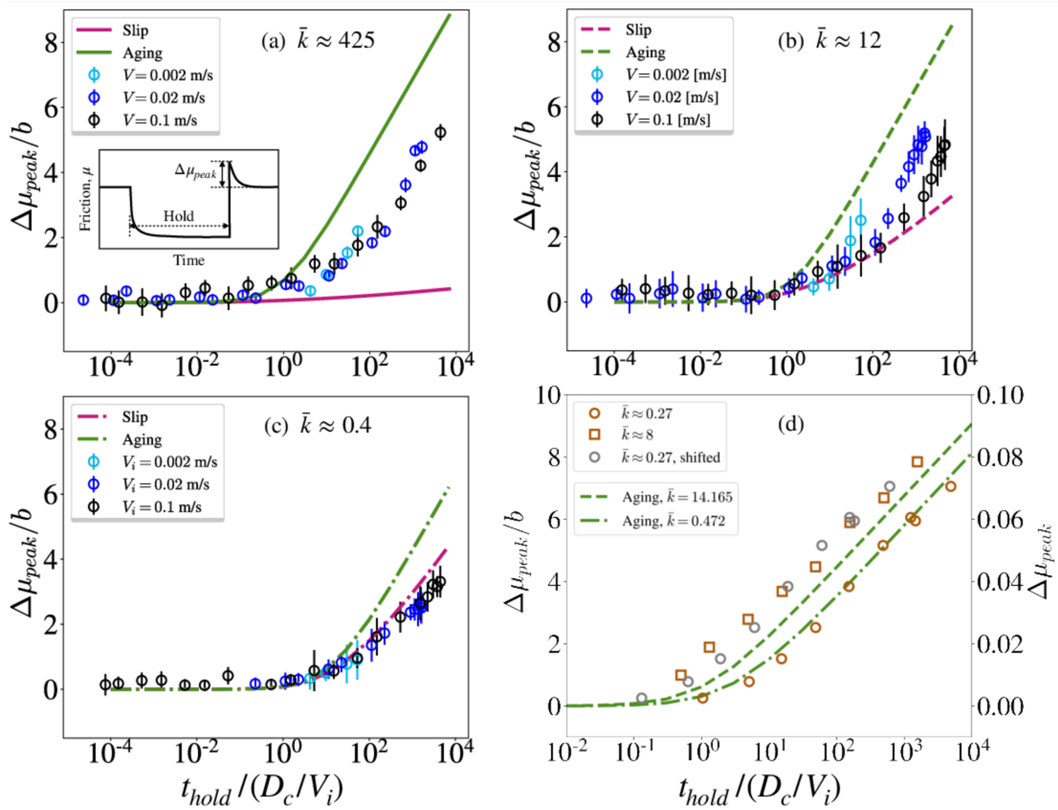

Figure 4. Frictional healing in the granular model: Solid circles show $\Delta\mu_{peak}$ normalized by the RSF parameter b (estimated from velocity steps), as a function of normalized hold time in granular slide-hold-slide simulations at $V_i = 2 \times 10^{-3}$, 2×10^{-2}, and 10^{-1} m/s. Panels (a), (b), and (c) show the results for system stiffnesses of $\bar{k}_d \approx 425$, 12, and 0.4, respectively. Error bars are 2-sigma deviations of 8 different realizations. The green and pink lines in each panel show the predictions of the Aging and Slip laws, respectively, for that specific system stiffness using the RSF parameters obtained from velocity-step tests. The inset in panel (a) shows the schematic of a slide-hold-slide test and the definition of frictional healing, $\Delta\mu_{peak}$. (d) Frictional healing in the lab: Solid circles show $\Delta\mu_{peak}$ as a function of normalized hold time, in slide-hold-slide experiments performed on a granite sample at 25 MPa confining pressure (Beeler et al., 1994) with machine stiffness $\bar{k}_d \approx 0.27$ and 8, at sliding velocities of $V_i = 1$ μm/s and 0.32 μm/s, respectively. The green dashed lines show the evolution of frictional healing, $\Delta\mu_{peak}$, normalized by the RSF parameter $b = 0.0109$ (estimated from the slope of healing vs. time data in this figure) with $a - b = -0.0027$ (Bhattacharya et al., 2017) and $D_c = 2$ μm (Bhattacharya et al., 2021). These parameters result in normalized stiffness values of $\bar{k}_d \approx 0.472$ and 14.165 for the Aging law predictions in this plot.

equations not captured by the standard RSF equations (1)–(3). However, over the same range of velocities Carpenter et al. (2016) found no significant dependence of the rate of healing upon V_i.

Here we present results of granular SHS simulations for a wide range of hold times at $V_i = 2 \times 10^{-3}$, 2×10^{-2}, and 10^{-1} m/s. Panels (a), (b) and (c) in Fig. 4 show the changes in peak stress with hold time for simulations performed with stiffnesses $\bar{k}_d \approx 425$, 12, and 0.4, respectively. These panels show that for the longest holds, the peak stress increases nearly logarithmically with hold time, in qualitative agreement with laboratory rock friction data. In each panel the green and red lines indicate the predictions of Aging and Slip law simulations, respectively, using parameter values determined from Slip law fits to our velocity-step simulations. For each stiffness (each panel) the slope of the green Aging-law prediction is equal to b, when plotted vs. $\ln(\bar{t}_{hold})$ rather than $\log_{10}(\bar{t}_{hold})$. Comparison to the granular simulations show that the slope of the log-time healing ranges from ∼0.5b to b, also in qualitative agreement with laboratory data. However, unlike the data of Beeler et al. (1994), the rate of healing at long hold times differs by nearly factor of 2 between the simulations with $\bar{k} \approx 12$ and $\bar{k} \approx 0.4$. In addition, unlike the data of Marone and Saffer (2015), but similar to that of Carpenter et al. (2016), there is not an obvious dependence of this slope upon V_i.

In contrast to the Aging law, the Slip law simulations produce a strongly stiffness-dependent rate of frictional healing. For $\bar{k} \approx 425$, there is so little slip that there is almost no state evolution (healing). For $\bar{k} \approx 0.4$, there is so much slip that the rate of healing is not much less than that for the Aging law. Note that the healing in the granular simulations is more than that predicted by the Slip law when $\bar{k}_d \approx 425$ and 12, but less than predicted when $\bar{k}_d \approx 0.4$. Thus, the observation of Ferdowsi and Rubin (2020) that for $\bar{k} \approx 425$ the healing in the granular model lies between the Aging and Slip law predictions is not generalizable to all stiffnesses.

The laboratory rock friction data of Beeler et al. (1994) are shown in Figure 4d. Only $(a - b)$ was determined in this study, so for the Aging law simulations shown we take $D_c = 2\mu$m determined for the same sample by Bhattacharya et al. (2021), and fix $b = 0.0109$ to match the slope of the lab healing curves. This comparison shows that while healing in the lab data leads that of the Aging law prediction (for the higher lab stiffness) or is in general agreement with it (for the lower stiffness), healing in the granular simulations generally lags the corresponding Aging-law prediction. This comparison should be extended to lab experiments where the RSF parameters were determined independently. A full comparison and discussion of how the RSF Aging and Slip laws perform in fitting the lab data of Beeler et al. (1994) are presented in section 3 of Bhattacharya et al. (2017), and we refer the interested reader to that work.

In laboratory slide-hold-slide experiments, the reslide is accompanied by dilation of the gouge layer, dilation that continues monotonically beyond the moment of peak stress to the future steady-state thickness. We observe the same behavior in our simulations. Figures 5a to 5c show the variation of dilation at peak stress in the granular model for the sliding velocities $V_i = 0.1$, 0.02, and 0.002 m/s, respectively, for each of the 3 stiffnesses we used. This dilation increases nearly linearly with log-hold time. For the simulations with $V_i = 0.1$ and 0.02, the magnitude of this dilation (at large normalized hold times) decreases with increasing system stiffness, opposite to the trend seen in the lab data of Beeler et al. (1994) and shown in Fig. 5d. The trend of the change in dilation at peak stress with system stiffness for the simulations with $V_i = 0.002$ m/s is in better agreement with the laboratory observations in Fig. 5d. We further normalize the dilation at peak stress by the amount of compaction at the end of the corresponding hold. The ratio of dilation/compaction that results from this analysis is shown in Fig. 5e, plotted alongside the same quantity observed in the lab data of Beeler et al. (1994). Comparing the lab data to the simulations conducted at roughly the same stiffnesses, we find that the relative slopes of the log-linear portion of the dilation and compaction in both the simulations and lab (normalized hold times $\gtrsim 10^1$) are in the fairly narrow range $\sim 0.4{-}0.5$, and are there therefore in qualitative agreement with each other. For shorter hold times, both the lab data and simulations show considerable scatter.

Among other features observed in slide-hold-slide tests, Figure 5 of Marone and Saffer (2015) suggests that the slip-weakening distance following the peak stress upon resliding increases with hold duration. This feature is inconsistent with the Slip law prediction, but we see evidence of similar behavior in our SHS simulations. Figures 6a & b show the variation of friction coefficient with sliding distance in the reslide portion of SHS simulations performed after a range of hold times, for $V_i = 0.1$ and 0.02 m/s, referenced to the steady-state friction value at V_i. These signals show (more obviously in Fig. 6a) that the slip distance to peak friction increases with increasing hold time, as for the Marone and Saffer (2015) data (their Figure 12). Panels c-d in Fig. 6 also include the Slip law prediction for a one-order velocity-step increase, normalized to the same peak-residual value as the reslide friction signals. These two panels more clearly demonstrate the increase in weakening distance with hold time. The reslides at shorter holds have a weakening distance, D_c, roughly equal to the distance observed in the velocity-steps. At longer hold times, D_c further increases, although

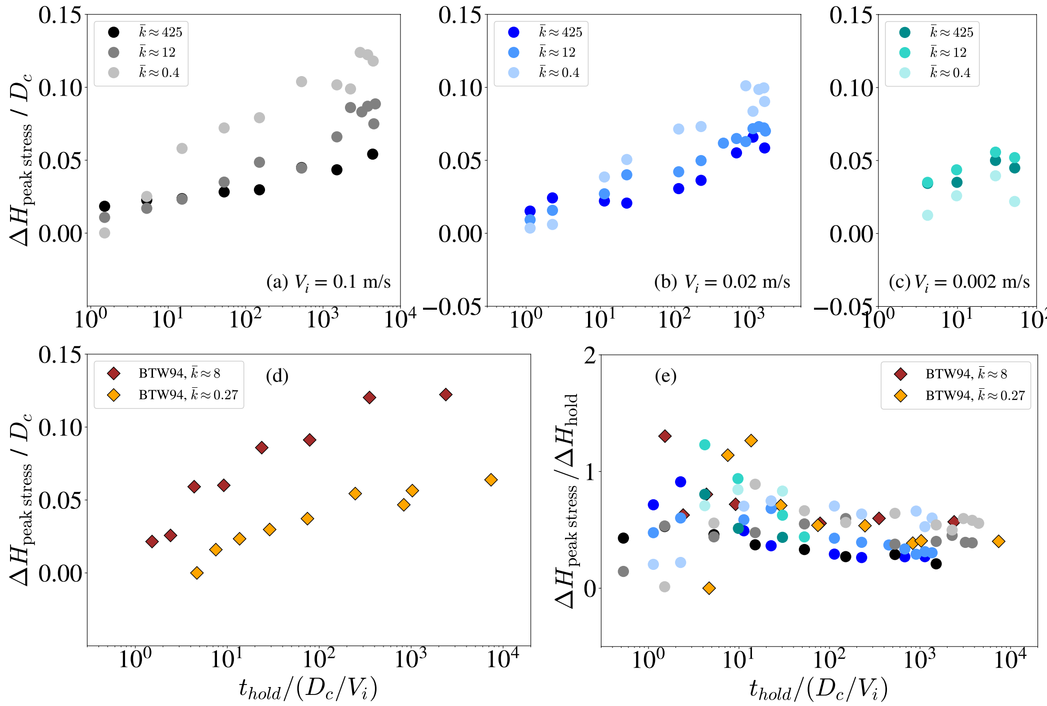

Figure 5. The variation of normalized dilation at peak stress ($\Delta H_{\text{peak stress}} / D_c$) versus hold time, following reslides for the granular model with sliding velocities of (a) $V_i = 0.1$ m/s, (b) $V_i = 0.02$ m/s, and (c) $V_i = 0.002$ m/s. The amount of dilation is defined as the change in gouge thickness between the end of the hold and the moment of peak stress, as in Fig. B1 of Bhattacharya et al. (2017). The simulations are performed at three different stiffnesses and 5 MPa confining stress. (d) dilation at peak stress ($\Delta H_{\text{peak stress}}$) in the lab (data of Beeler et al. (1994)), (e) The ratio of dilation at peak stress ($\Delta H_{\text{peak stress}}$) to compaction at the end of the corresponding hold in the granular model (circles) and in the lab (diamonds) (data of Beeler et al. (1994)). The lab data shown in panels (d) and (e) are reported by Bhattacharya et al. (2017).

the amount of increase in D_c in the granular model appears to be less than that observed in lab data. Sleep et al. (2000) proposed a model in which delocalization of slip within a granular layer during a hold led to an increase in the effective slip-weakening distance after a reslide, as slip gradually re-localized. If this explanation is correct, the relatively small increase in D_c that we observe could be due to the lack of obvious localization in our simulations.

In our SHS simulations, we have also investigated whether changing the re-sliding velocity changes either the peak friction or the approach to the future steady-state friction. Any behavior that deviates from the RSF prediction is relevant to models of earthquake nucleation, as the perimeter of an expanding nucleation zone subjects regions that have not slipped for a long time (as in a hold) to successively larger velocity jumps (Ampuero & Rubin, 2008). For this purpose, we have run reslide simulations after a hold time $\bar{t}_{hold} \sim 1650$, with the initial sliding velocity $V_i = 0.02$ m/s and reslide velocities V_r of 0.02, 0.05, 0.1, and 0.3 m/s. In a sense these are velocity-step tests, but run from a single value of state that is much larger than the steady-state value at velocity V_i. The results are shown in Fig. 7, where friction is plotted relative to its future steady-state value. The prediction of equation (1), assuming that the change in state between the end of the hold and peak stress is either small or independent of the reslide velocity, is that the difference in $\Delta\mu_{peak}$ between two reslide velocities V_2 and V_1 is equal to $b\ln(V_2/V_1)$. The inset in Fig. 7-a shows that this is very nearly the case, with $\Delta\mu_{peak}$ increasing linearly with $\ln(V_r/V_i)$ with a slope of 0.0155, or 87% of the value $b = 0.0178$ measured in velocity-steps. Furthermore, scaling the $\Delta\mu$ curves by the value

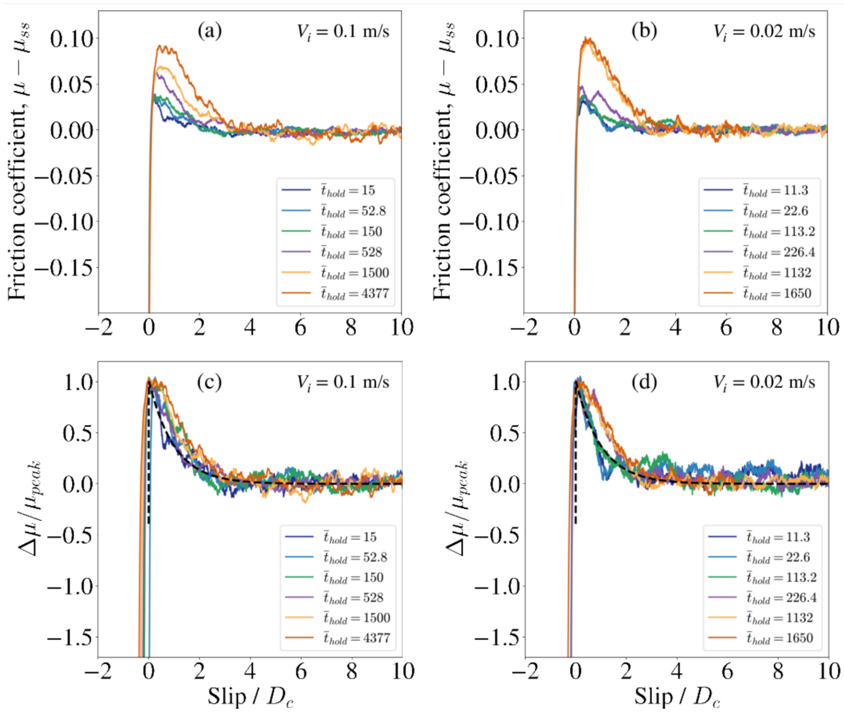

Figure 6. The variation of friction ($\mu - \mu_{ss}$) versus slip distance (Slip / D_c) during the reslide portion of slide-hold-slide simulations, for different values of normalized hold time $t_{hold}/(D_c/V_i)$ and sliding velocities of (a) $V_i = 0.1$ m/s and (b) $V_i = 0.02$ m/s. Panels (c) and (d) show the signals in panels (a) and (b) with values normalized by the peak friction value in each simulation. All simulations are performed with stiffness $\bar{k}_d \approx 425$ at 5 MPa confining stress. The black dashed line in panels (c) and (d) show the Slip law predictions for a one order of magnitude velocity-step increase, using the RSF parameters that provide good fits to velocity steps of various sizes performed with the granular model (Ferdowsi & Rubin, 2020). The Slip law prediction is scaled to the same peak-residual scale as the granular simulation data in the panels. The lines are added to show that the slip-weakening distance D_c increases with hold duration from a minimum value that is consistent with the value appropriate for velocity steps.

$[C + \ln(V_r/V_i)]$ in Fig. 7-b, with the value of $C = 5$ determined empirically (the value of $\Delta\mu_{peak}/b$ determined for $V_r = V_i$), collapses the frictional response for all the reslide velocities onto a single curve, consistent with the Slip law prediction. In other words, within the range of velocities that we have explored, changing the reslide velocity does not affect the weakening distance D_c in the granular model, consistent with the Slip law prediction, and changes the peak friction in accordance with standard RSF.

5 Energetics of granular slide-holds

Granular materials are non-equilibrium thermodynamic systems; as such, if the "effective thermodynamic temperature" of a granular system could be determined, this would allow extrapolating frameworks and relations from equilibrium thermodynamics to these systems. Although the exact definition of an effective temperature for granular materials is still a matter of much debate (Ono et al., 2002; Blumenfeld & Edwards, 2009; Puckett & Daniels, 2013; Bi et al., 2015; D. Richard et al., 2021), recent research results suggest that the fluctuating kinetic energy in these systems can play a role similar to the effective temperature. For this reason, the fluctuating kinetic energy (that is, the kinetic energy determined after subtracting from the velocity vector of each grain the average

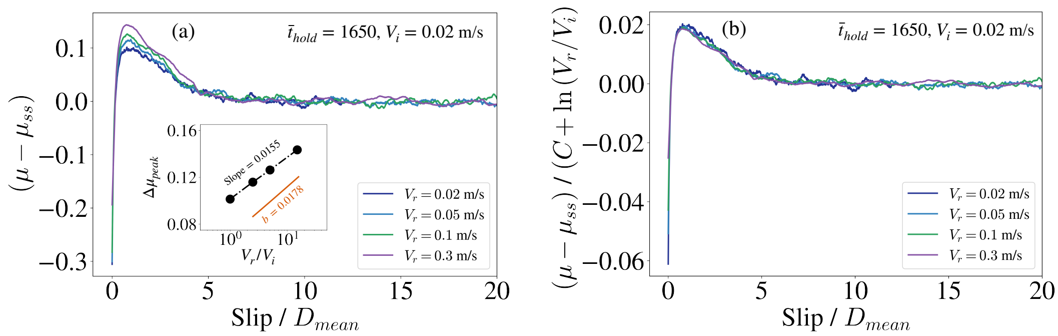

Figure 7. The variation of (a) friction $(\mu - \mu_{ss})$ versus slip distance (Slip / D_c), and (b) normalized friction $(\mu - \mu_{ss})/(C + \ln(V_r/V_i))$ versus slip distance (Slip / D_c), during reslide portion of slide-hold-slide simulations for normalized hold time $\bar{t}_{hold} \approx 1650$, with the initial sliding velocity, $V_i = 0.02$ m/s, and different reslide velocities, $V_r = 0.05$ m/s, 0.1, and 0.3 m/s. The value of $C \sim 5$ is chosen empirically. The inset in panel (a) shows the variation of peak friction $(\mu - \mu_{ss})_{peak}$ versus the ratio of reslide to initial velocity, V_r/V_i. All simulations are run with system stiffness $\bar{k}_d \approx 425$ at the confining stress 5 MPa.

velocity vector of all the grains in its immediate environment) is often referred to as the "granular temperature", and it has proven to be an important control on the rheological behavior of these systems (Campbell, 1990; Losert et al., 2000; Kim & Kamrin, 2020). In our previous work, we found that the magnitude of the RSF direct effect parameter a in the sheared granular gouge could plausibly be explained as the ratio of the fluctuating kinetic energy to the stored potential energy in the system (Ferdowsi & Rubin, 2020), although this proposal requires further investigation. We further showed that in the quasi-static shearing regime ($V \lesssim 1$ m/s, for a normal stress of 5 MPa), the fluctuating kinetic energy becomes nearly constant, which would suggest a nearly constant magnitude of the direct effect, consistent with most laboratory rock and gouge friction experiments (Kilgore et al., 1993; Bhattacharya et al., 2015). A nearly constant value of effective granular temperature in the quasi-static regime has also been previously reported in experimental granular physics studies (Song et al., 2005; Corwin et al., 2005), although more recent studies of granular systems with different loading geometries (i.e., other than tabular gouge layers between parallel plates) shows that this behavior could be influenced by localized deformation close to driving boundaries (Gaume et al., 2020; Kim & Kamrin, 2020; P. Richard et al., 2020).

In this work, we further examine the evolution of fluctuating kinetic energy in granular slide-hold simulations. The instantaneous per-grain fluctuating kinetic energy is defined in the tensorial form,

$$\boldsymbol{\delta E_k}(t) = \frac{1}{N} \sum_{i=1}^{N} m_i \delta\vec{v}_i(t) \otimes \delta\vec{v}_i(t), \tag{14}$$

where $\delta\vec{v}_i(t) = \vec{v}_i(t) - \vec{v}_i(z_k, t)$, m_i is the mass of the ith particle, and N is the total number of particles within the sheared granular layer. In these calculations, $\vec{v}_i(z_k, t)$ is the instantaneous linear velocity field, calculated with coarse-graining of the granular model data, according to $\vec{v}_i(z_k, t) = (1/N_k) \sum_{i=1}^{N_k} \vec{v}_i(t)$, in which $v_i(t)$ is the linear velocity of the ith particle within the rectangular cuboid with dimensions (L_x, L_y, $\Delta z = 1.37 D_{mean}$), and N_k is the total number of grains within each cuboid.

The variation of per grain fluctuating energy δE_k with hold time for slide-holds with initial sliding velocities $V_i = 0.1$ and 0.02 m/s and three different system stiffnesses are shown in Figs. 8a and 8b, respectively. The curves appear somewhat noisy because the individual data points are snapshots and not averages over some time window. The results show that with these two initial velocities, for moderate hold times δE_k decreases log-linearly over about 4 orders of magnitude in hold time, and then plateaus at roughly 50% of its initial steady-state value. Decreasing the system

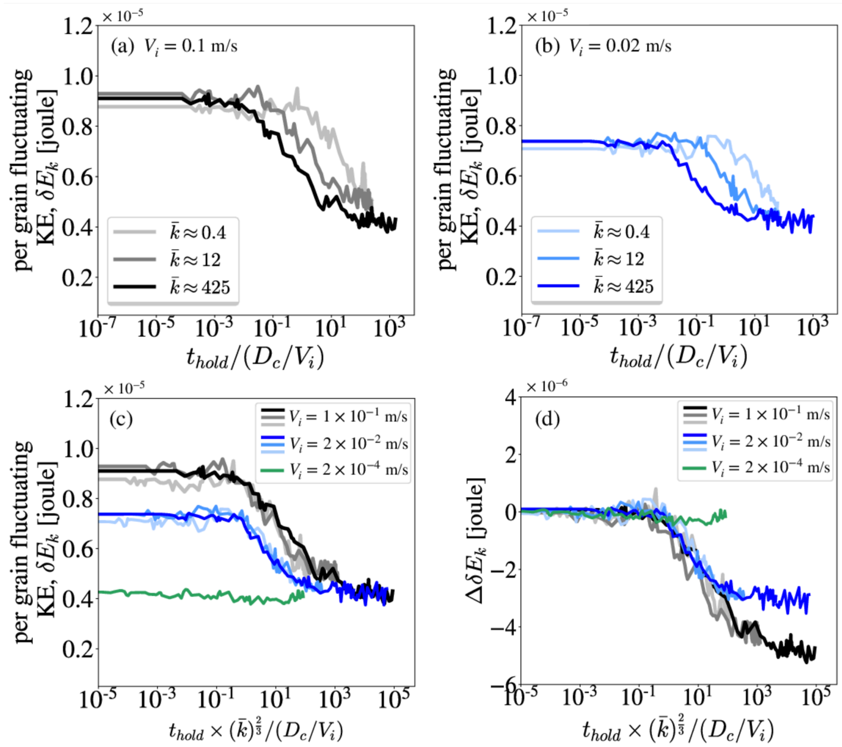

Figure 8. The variation of per grain fluctuating kinetic energy (δE_k) with hold time in slide-hold simulations performed with three system stiffnesses $\bar{k}_d \approx 425,\ 12,$ and 0.4, at two sliding velocities of (a) $V_i = 0.1$ m/s and (b) $V_i = 0.02$ m/s. (c) The variation of δE_k with (hold time)× (system stiffness, $\bar{k}_d)^{\frac{2}{3}}$ for all data shown in panels (a) and (b). (d) same as panel (c) with δE_k referenced to its initial value ($\delta E_{k,0}$) for each simulation. The green lines in panels (c) and (d) show the variation of δE_k and $\delta E_k - \delta E_{k,0}$ for simulations with sliding velocity $V_i = 2 \times 10^{-4}$ m/s and stiffness $\bar{k}_d \approx 425$. All simulations are performed at 5 MPa confining stress.

stiffness delays the onset of the reduction in δE_k, presumably because this allows stresses and sliding velocities near the prior steady state to persist for longer times, but does not otherwise change the shape of the energy reduction curves. This is shown by Fig. 8c, where for both V_i we further multiply the normalized hold time $\bar{t}_{hold}$ by $\bar{k}_d^{2/3}$, resulting in the collapse of all the simulation results for each initial velocity (at this point the choice of 2/3 for the power is strictly empirical). Plotting the change in δE_k from its initial steady state value further shows that the onset of the kinetic energy reduction is similar for both values of V_i (Figure 8d).

Figure 8c also shows that although the curves for the lower V_i have a slightly smaller δE_k at steady state ($\delta E_{k,ss}$), for all stiffnesses both V_i appear to plateau to the same value of δE_k at large hold times. This raises the question of whether there would be any reduction in δE_k during the hold for values of V_i small enough for $\delta E_{k,ss}$ to be at or below this plateau value. Ferdowsi and Rubin (2020) found that the steady-state value of δE_k decreased from about 1.7×10^{-5} J at $V = 10^{-1}$ m/s to slightly below 10^{-5} J at $V = 10^{-4}$ m/s (triangles in Figure 9b), close to the plateau value of δE_k in Figure 8c. For this reason we ran slide-hold simulations with $V = 2 \times 10^{-4}$ m/s, about the lowest value that could reach moderate values of $\bar{t}_{hold}$ in a reasonable amount of computation time (about 1.5 months). For the same reason the simulations were run only at the largest stiffness; this leads to the largest reduction in δE_k for a given $\bar{t}_{hold}$. We find that, indeed, δE_k for these simulations starts near the plateau value for the larger V_i in Figure 8c, and undergoes very little decay during the hold. Despite this, the stress decay, when plotted vs. dimensionless hold time, appears very similar to that for $V_i = 2 \times 10^{-2}$ and 10^{-1} m/s (Fig. 10. This result raises the possibility that the value of 0.8×10^{-5}

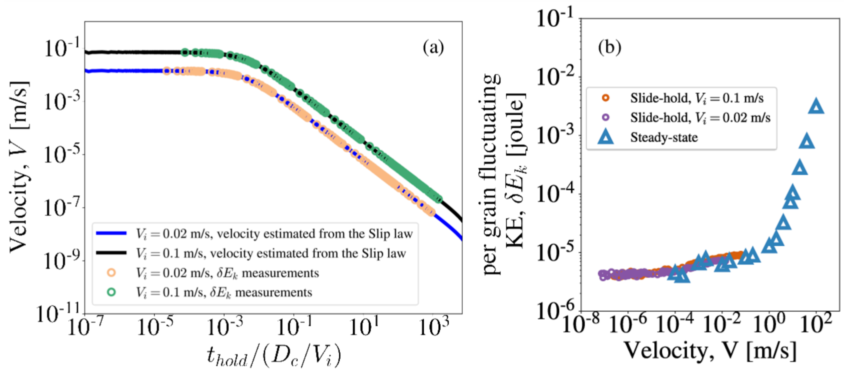

Figure 9. (a) Estimated sliding velocities during the slide-hold simulations with $\bar{k} \approx 425$ and initial sliding velocities $V_i = 0.02$ m/s and 0.1 m/s in Figure 2a (solid lines), and the times at which measurements of the per grain fluctuating kinetic energy (δE_k) were made (open circles), as functions of dimensionless hold time. Determining the slip speed directly from the simulations by taking the time-derivative of equation (4) (with $\delta_{lp} = 0$) results in very noisy velocity histories. Instead, we estimate the slip speed from the Slip law fit to these data. These estimated velocities equal the actual velocities whenever the simulations and the Slip law fit (solid red line in Figure 2a) have the same slope at the same value of t_{hold}. (b) The variation of per grain fluctuating kinetic energy with sliding velocity in the slide-hold simulations of panel (a) (magenta and brown circles) and in steady-state simulations reported in Ferdowsi and Rubin (2020) (blue triangles; the break in slope just below 1 m/s marks the boundary between the quasi-static and inertial regimes of flow). All simulations are performed at 5 MPa confining stress.

J for δE_k represents something of a floor for this granular system, as long as stresses are large enough to drive inelastic deformation. Because of the long computation times required we have been unable to explore this under conditions of steady-state sliding, but for the largest-stiffness holds in Figure 8, the velocities at the end of the simulations were $\sim 10^{-8} - 10^{-7}$ m/s for the different V_i (Fig. 9a). The variation of per grain fluctuation energy versus sliding velocity during holds follows closely the trend we have observed in the steady-state simulations, although it extends that trend to much lower velocities (Fig. 9b), and this suggests the sliding velocity is likely a primary factor in controlling the fluctuating energy, whether or not the system is at quasi-steady state.

We do not yet understand what controls the nearly fixed value of the fluctuating kinetic energy at long hold times or low steady-state sliding speeds in our simulations. For as long as δE_k is nearly constant, the energy loss from grain-grain friction and inelastic collisions must be balanced by work done on the gouge by the moving upper plate (or a reduction in elastic potential energy, but this is not an option during steady sliding, and even during holds, at constant confining pressure this strikes us as a less likely source). During load-point holds this work comes from both shearing (equivalent to the potential energy loss of the attached spring) and compaction. In these high-stiffness simulations the shearing and compaction velocities are of the same order of magnitude. As both decay roughly logarithmically with time during the hold, the rate of energy loss must also decay logarithmically with time. For our default restitution coefficient ϵ of ~0.98, collisions are nearly perfectly elastic and we presume that most of the energy loss is due to grain-grain friction. To explore the effect of increasing the collisional energy loss, we ran simulations with $\epsilon \sim 0.3$, for $\bar{k}_d \approx 12$. The results of these highly damped simulations are shown in Fig. 11. We find that the stress decay is nearly indistinguishable from that with the higher restitution coefficient (Figure 11a), and that while δE_k for the lower restitution coefficient is offset to lower values, the shape of the curve of fluctuating energy with hold time is not much different (Figure 11b). We conclude that within the range explored, the choice of restitution coefficient does not significantly influence the mechanical behavior of these

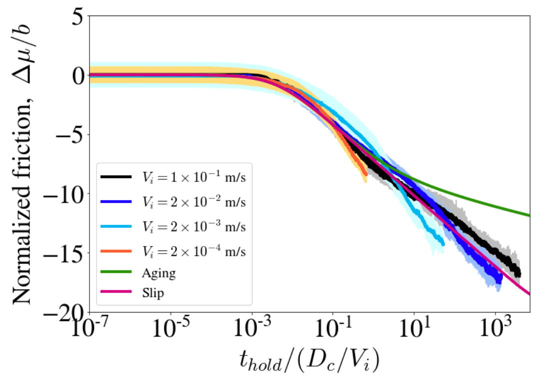

Figure 10. The variation of friction coefficient in slide-hold simulations with prior sliding velocities V_i of 2×10^{-4}, 2×10^{-3}, 2×10^{-2}, and 10^{-1} m/s. All simulations are run with system stiffness $\bar{k}_d \approx 425$ at the confining stress 5 MPa. The lines show the mean behavior of 8 realizations for each system, and the width of the shades regions around each line shows the 2-sigma deviations. The pink and green lines in panels (a) & (b) further show the predictions of the Slip and Aging laws, respectively, using the RSF parameters ($D_c = 0.0053$ m, $a = 0.0247$, $b = 0.0178$) determined independently from Slip-law fits to velocity-step tests performed on the same model (Ferdowsi and Rubin, 2020).

systems at such low strain rates, consistent with previous results (MiDi, 2004; Ferdowsi & Rubin, 2020).

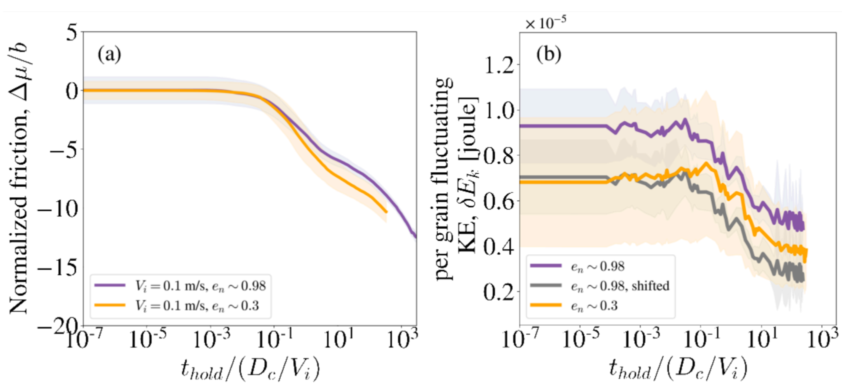

Figure 11. (a) The variation of friction coefficient, normalized by the RSF parameter b, as a function of normalized hold time, for granular slide-hold simulations with sliding velocity 10^{-1} m/s and two restitution coefficients of $\epsilon \sim 0.98$ and $\epsilon \sim 0.3$. (b) The variation of fluctuating kinetic energy with normalized hold time for the simulations in panel (a). The shaded regions indicate 2-σ standard deviations of 8 different realizations. The gray curve shows the fluctuating kinetic energy for the simulation with $\epsilon \sim 0.98$ shifted vertically.

If, as was proposed by Ferdowsi and Rubin (2020), the RSF direct effect parameter a is proportional to δE_k, then Figure 8 suggests that a might vary by a factor of ~2 over the duration of the holds with the larger V_i. One could then ask if the generally good fit of the Slip law, using constant parameter values, to the decay of friction during these same holds and to laboratory data, as in Figure 2, is really supportive of the Slip law for state evolution (that is, supportive of a model in which healing does not occur in the absence of slip). For example, is it possible that the friction data could be well fit by the Aging law (that is, by a model in which healing occurs with time even in the absence of slip), given the proper velocity-dependence of a? However, we note that for the highest-stiffness simulations in Figures 2 and 8, the continual log-linear stress decay continues to be well fit by the Slip law with constant parameter values even for dimensionless hold times larger than $\sim 10^{0.5}$, where δE_k is essentially constant. In addition, for the simulation with $V_i = 2 \times 10^{-4}$ m/s in Figure 10, δE_k is roughly constant and t_{hold} is arguably large enough to show that the friction data are more consistent with slip-dependent rather than time-dependent healing. We leave further investigation of the potential relation between measures of effective temperature and the value of a in granular simulations for future work.

6 Conclusions

In this work, we investigated the behavior of a sheared granular layer subjected to loading conditions designed to mimic laboratory slide-hold-slide experiments, for a range of sliding velocities and system stiffnesses. We compared the transient frictional behavior of the model to existing rock friction data, as well as to the predictions of standard rate-state friction (RSF) constitutive equations.

The behavior of the granular flow model in slide-hold simulations appears to closely resemble laboratory experiments in two important respects. First, the continual stress decay during the hold is reasonably well modeled by the Slip version of the RSF equations, using parameter values determined independently from velocity step tests on the identical system. This is consistent with lab data, as is the result that for both the granular simulations and lab data, the Aging version of the RSF equations predicts too little stress decay, a by-product of log-time healing (Bhattacharya et al., 2017, 2021). Second, in both the granular simulations and laboratory experiments, the fault layer undergoes compaction roughly linearly with log time. Even the rates are roughly comparable, at $\sim 0.05 D_c$ per decade of hold time in Figure 4. Log-time compaction is consistent with standard interpretations of the time-dependent Aging law for state evolution (compaction being a proxy for growth of true contact area), even though in both the granular simulations and lab experiments the stress decay is consistent with the Slip law and not the Aging law. As with the large velocity-step decreases described by Ferdowsi and Rubin (2020), this suggests a decoupling between state evolution and changes in fault or gouge thickness, in both the lab and the granular simulations, that seems inconsistent with traditional interpretations of RSF (Segall & Rice, 1995, e.g.).

The reslide portions of our granular slide-hold-slide simulations share with laboratory experiments the result that, for sufficiently long holds, the peak friction upon resliding ("frictional healing", $\Delta\mu_{peak}$) increases nearly linearly with the logarithm of hold time (J. H. Dieterich, 1972; Marone et al., 1990). For our maximum stiffness and larger lab-like stiffness ($\bar{k} \approx 12$), the long-time healing rate $d\Delta\mu_{peak}/d\ln(\bar{t}_{hold})$ is very close to the RSF evolution-effect parameter b, as predicted by the Aging law for all stiffnesses, but for our smaller lab-like stiffness ($\bar{k} \approx 0.4$) it is only half that value. The range of slopes we find is close to the range $\sim 0.3 - 0.7b$ seen in a study where the value of b was determined independently from velocity-step tests (Ikari et al., 2016; Carpenter et al., 2016). However, unlike the lab data of Beeler et al. (1994), we find this slope to be dependent upon the stiffness of the testing apparatus, by a factor of 2.

Thus, despite several shortcomings, including the use of spherical grains with a geologically narrow size distribution, and a range of sliding velocities that, due to computational expense, are very high by lab standards, it can still be argued that the granular model does a better job of matching laboratory experiments than existing, and empirical, rate-state friction equations. Unlike the comparison of velocity-step simulations to lab experiments emphasized by Ferdowsi and Rubin (2020), for the SHS protocols there are clearly some failures as well as successes of the granular model. It is entirely possible that some of these failures are due to time-dependent contact-scale processes in lab experiments that we specifically excluded from our simulations.

In our previous study, we evaluated the variation in fluctuating kinetic energy (δE_k) at steady-state shear velocities as low as 10^{-4} m/s, and found that δE_k becomes nearly-constant in quasi-static shear velocities (Ferdowsi & Rubin, 2020). In the slide-hold simulations reported here, we find that δE_k becomes even more nearly constant down to transient sliding velocities below 10^{-7} m/s. Further understanding what controls the changes in fluctuating kinetic energy, its near-constant value in the quasi-static limit, and its relation to the direct effect parameter a, may guide future studies of the proper formulations of rate-and-state friction laws for describing the transient frictional response of granular layers, and for connecting the RSF framework to more physics-based models.

Additional future research may explore recent definitions of state variable for amorphous materials (e.g., D. Richard et al. (2021)) in the context of elastoviscoplastic rheology for soft glassy materials (e.g., Fielding (2020)). Also, our study here has been focused on the stress relaxation and healing behavior of a sheared granular layer that shows velocity-strengthening frictional behavior. It has been recently observed that, even without implementing any sophisticated or time-dependent grain-contact scale processes in granular simulations, granular models that use certain grain shapes (Salerno et al., 2018), or grain-grain contact potentials/laws in certain regions of normal pressure and grain stiffness (such as the Hookean contact law, in the grain strain range smaller than 10^{-3} (Kim & Kamrin, 2020; DeGiuli & Wyart, 2017)) show velocity-weakening friction in the dense quasi-static flow regime. Exploring the transient rheology of such velocity-weakening systems in velocity-step and slide-hold-slide protocols, may provide more insights into the physics of granular rate-state behavior, and additional opportunities for comparing the behavior of the granular model to lab data when both are in the velocity-weakening regime of friction.

Acknowledgments

BF acknowledges support from the Department of Geosciences, Princeton University, in form of a Harry H. Hess postdoctoral fellowship. Research was sponsored by the US National Science Foundation (NSF) awards EAR-1547286 and EAR-1946434, by the US Geological Survey (USGS), Department of the Interior, awards G19AP00048 and G20AP00112, and by the US Army Research Office (ARO) award W911NF-20-1-0154, all of the awards to AMR. The authors thank Pathikrit Bhattacharya, Terry E. Tullis, Nicholas M. Beeler, and Keishi Okazaki, for their permission to use the data shown in Figure 2d of this manuscript. Parallel programs were run on computers provided by the Princeton Institute for Computational Science and Engineering (PICSciE). The 3-D visualizations of the model were performed using the open-source visualization software "The Persistence of Vision Raytracer" POV-Ray (http://www.povray.org). Most of the data analysis were carried out using the open-source Python library, NumPy (https://numpy.org). The 2-D plots were made with the Python library Matplotlib (www.matplotlib.org). The computer codes for LAMMPS simulations of this paper with the information about the version of LAMMPS used for the simulations, are available on the Dryad digital repository at *https://doi.org/10.5061/dryad.2z34tmphk*. The authors wish to thank reviewers Jianye Chen and Norm Sleep, and the Associate Editor, for their reviews and suggestions which helped improve and clarify this manuscript. The views and conclusions contained in this document are those of the authors and should not be interpreted as necessarily representing the official policies, either expressed or implied, of the U.S. Government.

References

Abe, S., Dieterich, J. H., Mora, P., & Place, D. (2002). Simulation of the influence of rate-and state-dependent friction on the macroscopic behavior of complex fault zones with the lattice solid model. *pure and applied geophysics*, *159*(9), 1967–1983.

Abe, S., & Mair, K. (2009). Effects of gouge fragment shape on fault friction: New 3d modelling results. *Geophysical Research Letters*, *36*(23).

Ampuero, J.-P., & Rubin, A. M. (2008). Earthquake nucleation on rate and state faults–aging and slip laws. *Journal of Geophysical Research: Solid Earth*, *113*(B1).

Baumberger, T., Berthoud, P., & Caroli, C. (1999). Physical analysis of the state-and rate-dependent friction law. ii. dynamic friction. *Physical Review B*, *60*(6), 3928.

Baumberger, T., & Caroli, C. (2006). Solid friction from stick–slip down to pinning and aging. *Advances in Physics*, *55*(3-4), 279–348.

Beeler, N., Tullis, T., Blanpied, M., & Weeks, J. (1996). Frictional behavior of large displacement experimental faults. *Journal of Geophysical Research: Solid Earth*, *101*(B4), 8697–8715.

Beeler, N., Tullis, T., & Weeks, J. (1994). The roles of time and displacement in the evolution effect

in rock friction. *Geophysical Research Letters*, *21*(18), 1987–1990.
Berthoud, P., Baumberger, T., G'sell, C., & Hiver, J.-M. (1999). Physical analysis of the state-and rate-dependent friction law: Static friction. *Physical review B*, *59*(22), 14313.
Bhattacharya, P., Rubin, A. M., Bayart, E., Savage, H. M., & Marone, C. (2015). Critical evaluation of state evolution laws in rate and state friction: Fitting large velocity steps in simulated fault gouge with time-, slip-, and stress-dependent constitutive laws. *Journal of Geophysical Research: Solid Earth*, *120*(9), 6365–6385.
Bhattacharya, P., Rubin, A. M., & Beeler, N. M. (2017). Does fault strengthening in laboratory rock friction experiments really depend primarily upon time and not slip? *Journal of Geophysical Research: Solid Earth*.
Bhattacharya, P., Rubin, A. M., Tullis, T. E., Beeler, N. M., & Okazaki, K. (2021). The evolution of rock friction is more sensitive to slip than elapsed time, even at near-zero slip rates. *Earth and Space Science Open Archive*. Retrieved from `https://doi.org/10.1002/essoar.10507717.1` doi: 10.1002/essoar.10507717.1
Bi, D., Henkes, S., Daniels, K. E., & Chakraborty, B. (2015). The statistical physics of athermal materials. *Annu. Rev. Condens. Matter Phys.*, *6*(1), 63–83.
Blanpied, M., Marone, C., Lockner, D., Byerlee, J., & King, D. (1998). Quantitative measure of the variation in fault rheology due to fluid-rock interactions. *Journal of Geophysical Research: Solid Earth*, *103*(B5), 9691–9712.
Blumenfeld, R., & Edwards, S. F. (2009). On granular stress statistics: Compactivity, angoricity, and some open issues. *The Journal of Physical Chemistry B*, *113*(12), 3981–3987.
Brilliantov, N. V., Spahn, F., Hertzsch, J.-M., & Pöschel, T. (1996). Model for collisions in granular gases. *Physical review E*, *53*(5), 5382.
Campbell, C. S. (1990). Rapid granular flows. *Annual Review of Fluid Mechanics*, *22*(1), 57–90.
Carpenter, B. M., Ikari, M. J., & Marone, C. (2016). Laboratory observations of time-dependent frictional strengthening and stress relaxation in natural and synthetic fault gouges. *Journal of Geophysical Research: Solid Earth*, *121*(2), 1183–1201.
Chen, J., & Spiers, C. J. (2016). Rate and state frictional and healing behavior of carbonate fault gouge explained using microphysical model. *Journal of Geophysical Research: Solid Earth*, *121*(12), 8642–8665.
Chen, J., van den Ende, M. P., & Niemeijer, A. R. (2020). Microphysical model predictions of fault restrengthening under room-humidity and hydrothermal conditions: From logarithmic to power-law healing. *Journal of Geophysical Research: Solid Earth*, *125*(4), e2019JB018567.
Corwin, E. I., Jaeger, H. M., & Nagel, S. R. (2005). Structural signature of jamming in granular media. *Nature*, *435*(7045), 1075.
da Cruz, F., Emam, S., Prochnow, M., Roux, J.-N., & Chevoir, F. (2005). Rheophysics of dense granular materials: Discrete simulation of plane shear flows. *Physical Review E*, *72*(2), 021309.
DeGiuli, E., & Wyart, M. (2017). Friction law and hysteresis in granular materials. *Proceedings of the National Academy of Sciences*, *114*(35), 9284–9289.
Dieterich, J. (1994). A constitutive law for rate of earthquake production and its application to earthquake clustering. *Journal of Geophysical Research: Solid Earth*, *99*(B2), 2601–2618.
Dieterich, J. H. (1972). Time-dependent friction in rocks. *Journal of Geophysical Research*, *77*(20), 3690–3697.
Dieterich, J. H. (1978). Time-dependent friction and the mechanics of stick-slip. In *Rock friction and earthquake prediction* (pp. 790–806). Springer.
Dieterich, J. H. (1979). Modeling of rock friction: 1. experimental results and constitutive equations. *Journal of Geophysical Research: Solid Earth*, *84*(B5), 2161–2168.
Dieterich, J. H. (1992). Earthquake nucleation on faults with rate-and state-dependent strength. *Tectonophysics*, *211*(1-4), 115–134.
Dieterich, J. H., & Kilgore, B. (1996). Implications of fault constitutive properties for earthquake prediction. *Proceedings of the National Academy of Sciences*, *93*(9), 3787–3794.
Dieterich, J. H., & Kilgore, B. D. (1994). Direct observation of frictional contacts: New insights for state-dependent properties. *Pure and Applied Geophysics*, *143*(1), 283–302.
Dieterich, J. H., et al. (1981). Constitutive properties of faults with simulated gouge. *Mechanical Behavior of*.

Ferdowsi, B., & Rubin, A. M. (2020). A granular-physics-based view of fault friction experiments. *Journal of Geophysical Research: Solid Earth*, e2019JB019016.

Fielding, S. M. (2020). Elastoviscoplastic rheology and aging in a simplified soft glassy constitutive model. *Journal of Rheology*, *64*(3), 723–738.

Forterre, Y., & Pouliquen, O. (2008). Flows of dense granular media. *Annu. Rev. Fluid Mech.*, *40*, 1–24.

Frye, K. M., & Marone, C. (2002). Effect of humidity on granular friction at room temperature. *Journal of Geophysical Research: Solid Earth*, *107*(B11), ETG–11.

Gaume, J., Chambon, G., & Naaim, M. (2011). Quasistatic to inertial transition in granular materials and the role of fluctuations. *Physical Review E*, *84*(5), 051304.

Gaume, J., Chambon, G., & Naaim, M. (2020). Microscopic origin of nonlocal rheology in dense granular materials. *Physical Review Letters*, *125*(18), 188001.

Handwerger, A. L., Rempel, A. W., Skarbek, R. M., Roering, J. J., & Hilley, G. E. (2016). Rate-weakening friction characterizes both slow sliding and catastrophic failure of landslides. *Proceedings of the National Academy of Sciences*, *113*(37), 10281–10286.

Hatano, T. (2009). Scaling of the critical slip distance in granular layers. *Geophysical Research Letters*, *36*(18).

Ikari, M. J., Carpenter, B. M., & Marone, C. (2016). A microphysical interpretation of rate-and state-dependent friction for fault gouge. *Geochemistry, Geophysics, Geosystems*, *17*(5), 1660–1677.

Johnson, K. L. (1987). *Contact mechanics*. Cambridge University Press.

Kato, N., & Tullis, T. E. (2001). A composite rate-and state-dependent law for rock friction. *Geophysical research letters*, *28*(6), 1103–1106.

Kilgore, B. D., Blanpied, M. L., & Dieterich, J. H. (1993). Velocity dependent friction of granite over a wide range of conditions. *Geophysical Research Letters*, *20*(10), 903–906.

Kim, S., & Kamrin, K. (2020, Aug). Power-law scaling in granular rheology across flow geometries. *Phys. Rev. Lett.*, *125*, 088002. Retrieved from `https://link.aps.org/doi/10.1103/PhysRevLett.125.088002` doi: 10.1103/PhysRevLett.125.088002

Landau, L. D., & Lifshitz, E. M. (1959). Theory of elasticity.

Li, Q., Tullis, T. E., Goldsby, D., & Carpick, R. W. (2011). Frictional ageing from interfacial bonding and the origins of rate and state friction. *Nature*, *480*(7376), 233.

Liu, Y., & Szlufarska, I. (2012). Chemical origins of frictional aging. *Physical review letters*, *109*(18), 186102.

Losert, W., Bocquet, L., Lubensky, T., & Gollub, J. P. (2000). Particle dynamics in sheared granular matter. *Physical review letters*, *85*(7), 1428.

Marone, C. (1998). Laboratory-derived friction laws and their application to seismic faulting. *Annual Review of Earth and Planetary Sciences*, *26*(1), 643–696.

Marone, C., Raleigh, C. B., & Scholz, C. (1990). Frictional behavior and constitutive modeling of simulated fault gouge. *Journal of Geophysical Research: Solid Earth*, *95*(B5), 7007–7025.

Marone, C., & Saffer, D. (2015). The mechanics of frictional healing and slip instability during the seismic cycle. In G. Schubert (Ed.), *Treatise on geophysics (second edition)* (Second Edition ed., p. 111 - 138). Oxford: Elsevier. Retrieved from `http://www.sciencedirect.com/science/article/pii/B9780444538024000920` doi: https://doi.org/10.1016/B978-0-444-53802-4.00092-0

McCarthy, C., Savage, H., & Nettles, M. (2017). Temperature dependence of ice-on-rock friction at realistic glacier conditions. *Philosophical Transactions of the Royal Society A: Mathematical, Physical and Engineering Sciences*, *375*(2086), 20150348.

MiDi, G. (2004). On dense granular flows. *European Physical Journal E–Soft Matter*, *14*(4).

Mindlin, R. D. (1949). Compliance of elastic bodies in contact. *J. Appl. Mech., ASME*, *16*, 259–268.

Morgan, J. K. (2004). Particle dynamics simulations of rate-and state-dependent frictional sliding of granular fault gouge. In *Computational earthquake science part i* (pp. 1877–1891). Springer.

Nagata, K., Nakatani, M., & Yoshida, S. (2012). A revised rate-and state-dependent friction law obtained by constraining constitutive and evolution laws separately with laboratory data. *Journal of Geophysical Research: Solid Earth*, *117*(B2).

Nakatani, M. (1998). A new mechanism of slip weakening and strength recovery of friction associated with the mechanical consolidation of gouge. *Journal of Geophysical Research: Solid Earth*, *103*(B11), 27239–27256.

Nakatani, M. (2001). Conceptual and physical clarification of rate and state friction: Frictional sliding as a thermally activated rheology. *Journal of Geophysical Research: Solid Earth*, *106*(B7), 13347–13380.

Ono, I. K., O'Hern, C. S., Durian, D. J., Langer, S. A., Liu, A. J., & Nagel, S. R. (2002). Effective temperatures of a driven system near jamming. *Physical review letters*, *89*(9), 095703.

Plimpton, S. (1995). Fast parallel algorithms for short-range molecular dynamics. *Journal of computational physics*, *117*(1), 1–19.

Puckett, J. G., & Daniels, K. E. (2013). Equilibrating temperaturelike variables in jammed granular subsystems. *Physical Review Letters*, *110*(5), 058001.

Rice, J. R. (2006). Heating and weakening of faults during earthquake slip. *Journal of Geophysical Research: Solid Earth*, *111*(B5).

Rice, J. R., & Cocco, M. (2007). Seismic fault rheology and earthquake dynamics. *Tectonic faults: Agents of change on a dynamic earth*, 99–137.

Rice, J. R., Lapusta, N., & Ranjith, K. (2001). Rate and state dependent friction and the stability of sliding between elastically deformable solids. *Journal of the Mechanics and Physics of Solids*, *49*(9), 1865–1898.

Richard, D., Kapteijns, G., Giannini, J. A., Manning, M. L., & Lerner, E. (2021, Jan). Simple and broadly applicable definition of shear transformation zones. *Phys. Rev. Lett.*, *126*, 015501. Retrieved from `https://link.aps.org/doi/10.1103/PhysRevLett.126.015501` doi: 10.1103/PhysRevLett.126.015501

Richard, P., Artoni, R., Valance, A., & Delannay, R. (2020). Influence of lateral confinement on granular flows: comparison between shear-driven and gravity-driven flows. *Granular Matter*, *22*(4), 1–13.

Ruina, A. (1983). Slip instability and state variable friction laws. *Journal of Geophysical Research: Solid Earth (1978–2012)*, *88*(B12), 10359–10370.

Salerno, K. M., Bolintineanu, D. S., Grest, G. S., Lechman, J. B., Plimpton, S. J., Srivastava, I., & Silbert, L. E. (2018). Effect of shape and friction on the packing and flow of granular materials. *Physical Review E*, *98*(5), 050901.

Segall, P., & Rice, J. R. (1995). Dilatancy, compaction, and slip instability of a fluid-infiltrated fault. *Journal of Geophysical Research: Solid Earth*, *100*(B11), 22155–22171.

Silbert, L. E., Ertaş, D., Grest, G. S., Halsey, T. C., Levine, D., & Plimpton, S. J. (2001). Granular flow down an inclined plane: Bagnold scaling and rheology. *Physical Review E*, *64*(5), 051302.

Sleep, N. H. (1995). Ductile creep, compaction, and rate and state dependent friction within major fault zones. *Journal of Geophysical Research: Solid Earth*, *100*(B7), 13065–13080.

Sleep, N. H. (1997). Application of a unified rate and state friction theory to the mechanics of fault zones with strain localization. *Journal of Geophysical Research: Solid Earth*, *102*(B2), 2875–2895.

Sleep, N. H. (2006). Real contacts and evolution laws for rate and state friction. *Geochemistry, Geophysics, Geosystems*, *7*(8).

Sleep, N. H., Richardson, E., & Marone, C. (2000). Physics of friction and strain rate localization in synthetic fault gouge. *Journal of Geophysical Research: Solid Earth*, *105*(B11), 25875–25890.

Song, C., Wang, P., & Makse, H. A. (2005). Experimental measurement of an effective temperature for jammed granular materials. *Proceedings of the National Academy of Sciences*, *102*(7), 2299–2304.

Thom, C., Carpick, R., & Goldsby, D. (2018). Constraints on the physical mechanism of frictional aging from nanoindentation. *Geophysical Research Letters*, *45*(24), 13–306.

Tian, K., Goldsby, D. L., & Carpick, R. W. (2018). Rate and state friction relation for nanoscale contacts: Thermally activated prandtl-tomlinson model with chemical aging. *Physical Review Letters*, *120*(18), 186101.

Tian, K., Gosvami, N. N., Goldsby, D. L., Liu, Y., Szlufarska, I., & Carpick, R. W. (2017). Load

and time dependence of interfacial chemical bond-induced friction at the nanoscale. *Physical review letters*, *118*(7), 076103.
Tse, S. T., & Rice, J. R. (1986). Crustal earthquake instability in relation to the depth variation of frictional slip properties. *Journal of Geophysical Research: Solid Earth*, *91*(B9), 9452–9472.
Viesca, R. C. (2016). Self-similar slip instability on interfaces with rate-and state-dependent friction. *Proceedings of the Royal Society A: Mathematical, Physical and Engineering Sciences*, *472*(2192), 20160254.
Zhang, H., & Makse, H. (2005). Jamming transition in emulsions and granular materials. *Physical Review E*, *72*(1), 011301.